PHYSICAL REVIEW D **78,** 093005 (2008)

$b\bar{b}H$ production at the CERN LHC: Yukawa corrections and the leading Landau singularity

F. Boudjema and Duc Ninh Le

LAPTH, Université de Savoie, CNRS, BP 110, F-74941 Annecy-le-Vieux Cedex, France

(Received 22 June 2008; published 7 November 2008)

At tree-level Higgs production in association with a b-quark pair proceeds through the small Yukawa bottom coupling in the standard model. Even in the limit where this coupling vanishes, electroweak one-loop effects, through the top-Higgs Yukawa coupling, in particular, can still trigger this reaction. This contribution is small for Higgs masses around 120 GeV but it quickly picks up for higher Higgs masses especially because the one-loop amplitude develops a leading Landau singularity and new thresholds open up. These effects can be viewed as the production of a pair of top quarks which rescatter to give rise to Higgs production through WW fusion. We study the leading Landau singularity in detail. Since this singularity is not integrable when the one-loop amplitude is squared, we regulate the cross section by taking into account the width of the internal top and W particles. This requires that we extend the usual box one-loop function to the case of complex masses. We show how this can be implemented analytically in our case. We study in some detail the cross section at the CERN LHC as a function of the Higgs mass and show how some distributions can be drastically affected compared to the tree-level result.

DOI: 10.1103/PhysRevD.78.093005 PACS numbers: 14.80.Bn, 12.15.Lk

I. INTRODUCTION

The CERN LHC will soon start running and collecting data. Although one expects surprises, discovering the Higgs is the highest priority. A lot of effort has gone in calculating the rate of production of this particle, within the standard model and beyond, for a host of channels and signatures; see [1,2] for a review.

Higgs production in association with a pair of bottom quarks is not, especially in the standard model, a discovery channel since the coupling of the Higgs to the bottom quark is given by the small, $\mathcal{O}(m_b/v)$ bottom-Higgs Yukawa coupling, where m_b is the bottom mass and $v \sim 246$ GeV is the scale of electroweak symmetry breaking. Nonetheless, given the special role that can play the third generation of fermions in the mechanism of symmetry breaking and, in particular, the top-bottom quark doublet, a reconstruction of this Higgs coupling to bottom quarks is important. This reconstruction and interpretation of the measurements requires theoretical predictions that go beyond the tree-level approximation. Many of these calculations, most of which concern the important QCD corrections, have already been performed [3]. Usually one expects the electroweak corrections to be small and not compete with the QCD corrections. However, one should bear in mind that the top Yukawa coupling $\mathcal{O}(m_t/v)$ is of order the strong coupling constant. If this coupling takes part in the electroweak corrections the latter may not necessarily be small. Other Yukawa couplings that are not negligible are the Higgs Yukawa coupling.[1] Both these couplings are involved when one considers the electroweak corrections to $b\bar{b}H$ production at the LHC. Another important property of the electroweak effects is that this cross section can be triggered off by one-loop corrections involving the top quark and W gauge boson (or Goldstone) loops even for vanishing $b\bar{b}H$ (or $m_b = 0$) coupling, where the Born cross section vanishes.

We [4] have, very recently, studied the effects of the leading (Yukawa-type) electroweak corrections for $b\bar{b}H$ production at the LHC in a situation where both b's are tagged, requiring somewhat large p_T b, as would be relevant for a measurement of the $b\bar{b}H$ couplings and a complete identification of this channel. The study we performed concentrated on a Higgs with a mass below 150 GeV not only because this range is preferred by the precision electroweak data but also because the cross section decreases much with increasing Higgs mass. It was found that, after all, the next-to-leading order (NLO) corrections were small and could be safely neglected. In the limit where the $b\bar{b}H$ coupling vanishes and where the cross section is induced solely through electroweak loops, we found that this effect is much larger than the NLO correction and increases rapidly with the Higgs mass. We pointed out that, for this contribution, as $M_H \geq 2M_W$ our perturbative calculation becomes unreliable since the loop integrals start showing numerical instabilities. We had identified this behavior as a leading Landau singularity (LLS) [5,6] which is a pinch singularity of the loop integral. This, in part, has an interesting physical origin: the on shell production and rescattering of the top quarks into on shell W bosons, the latter giving rise to Higgs production through WW boson fusion. This LLS of the one-loop four-point function is not integrable when one considers the square of the loop amplitude as needed for vanishing $b\bar{b}H$ coupling. The NLO contribution, on the other hand, is integrable.

[1] As this paper is on the Yukawa corrections neglecting corrections of order the electroweak gauge coupling, we use the terminology *Higgs Yukawa coupling* for the Higgs self-coupling which in the standard model is not a gauge coupling.

The aim of this paper is to extend the study we made in [4] to higher Higgs masses. The emphasis will be on the LLS problem and the pure one-loop contribution in the limit of vanishing m_b since this is the major hurdle. For completeness we will also give results for the NLO contribution for Higgs masses not covered in our previous calculation. Beyond the phenomenological impact of the LLS for the case at hand, the study of the LLS in this paper should be of interest for other situations considering that one rarely encounters such singularities, as compared to the inverse (vanishing) Gram determinant which is not a genuine physical singularity but an artifact of the reduction of the tensorial integrals. Some of the few examples in the relatively recent literature where some aspect of a Landau singularity shows up include $ZZ \to ZZ$ [7] and the 6-photon amplitude [8] in the standard model both with massless particles in the internal states involving a four-point function. Beyond the standard model we can mention loop corrections to sfermion pair production in supersymmetry [9] and Higgs production from the decay of a fourth-generation b-like quark [10], both these examples involve heavy instable particles in a three-point function. In [9], no special treatment of the singularity is required since the study is made at the NLO level where this singularity is integrable. In [10], the width of the internal unstable particle is called for. In $ZZ \to ZZ$, the study [7] keeps away from the region of the LLS, while it is argued that the LLS should disappear if one considers a more inclusive cross section where the Z boson would decay or the initial Z are grafted to light stable fermions. For the case of the 6-photon amplitude the situation is quite subtle. The QED dynamics is such that the LLS disappears at the level of the total gauge invariant amplitude after summing on individual diagrams. The LLS issue can also be relevant for the nascent *cut techniques* of computing loop amplitudes; for a recent review see [11]. This is the reason we devote a fair part of this paper to the study and solution of the LLS. Our solution to the problem of the LLS for Higgs production through $gg \to b\bar{b}H$ is to endow the resonating internal particles, namely, the top quark and W gauge boson with a width. The extension of the usual loop libraries, such as FF [12] of LOOPTOOLS [13], to the case of complex masses is not trivial especially if one insists on an analytical implementation. We will show how the case at hand lends itself to a fairly manageable implementation of complex masses for the four-point function which is computer-time effective. The introduction of the widths avoids all numerical instabilities and smooths out the cross section when we enter the phase-space region of the LLS. It rests that this effect can still give large corrections particularly for some specific distributions, like, for example, the p_T distribution of the bottom quark or the Higgs boson.

The plan of the paper is as follows. In the next section we set the framework for our calculation with a reminder on the $SU(3)$ (QCD) gauge invariant classes of the electroweak contributions and the helicity properties of the amplitudes. We then briefly uncover the class and type of diagrams that contain a potential leading Landau singularity. Section III follows with a general discussion on the Landau singularities first exposing the conditions under which such singularities can show up for the scalar N-point function. We then carefully extract the nature of the singularity before moving into a detailed investigation of the scalar four-point function at the origin of the LLS in our case, for $gg \to b\bar{b}H$. Section IV discusses how this singularity can be regulated through taking into account the width of the unstable particles running in the loop. Section V describes how these widths are implemented through a modification of the loop integrals that should be defined for complex masses of the loop particles. In particular we describe our analytical implementation of the complex masses suitable for our problem. We will also discuss the various checks we made to insure the correctness of the implementation. Section VI gives briefly our input parameters and cuts and describe how the cross section at the pp level is obtained. Section VII gives our main results for the cross section $pp \to b\bar{b}H$ at the LHC in the limit of vanishing Higgs coupling to b-quarks. In this case, the cross section is induced at one-loop and we need, in particular, to integrate the square of the four-point loop integral over the kinematical phase space. This calls for our new implementation of the box one-loop functions. We will discuss the behavior of the cross section as a function of the Higgs mass and study a few distributions. Section VIII turns to the NLO result for $M_H > 150$ GeV, completing therefore the study we made in [4]. Section IX summarizes our findings. The paper contains also three appendices. In the first, we give the details of our derivation of the nature of the singularity while the second appendix gives technical details about the handling of complex masses in one-loop scalar box functions. The third appendix details the singularities of the three-point function. Many key issues about the LLS are unravelled in this case which help in better understanding the issues in the four-point function.

II. A QUICK REMINDER AND GENERAL CONSIDERATIONS OF THE ONE-LOOP ELECTROWEAK STRUCTURE

At LHC energies the exclusive $b\bar{b}H$ production with both b-quarks tagged is dominated, by far, by the gluon-gluon initiated subprocess. We therefore only consider, as we have done in [4], the gluon-gluon initiated subprocess $g(p_1, \lambda_1) + g(p_2, \lambda_2) \to b(p_3, \lambda_3) + \bar{b}(p_4, \lambda_4) + H(p_5)$. $\lambda_i = \pm$ and p_i with $i = 1, 2, 3, 4$ stand for the helicity for the momentum of the particle. The corresponding helicity amplitude will be denoted as $\mathcal{A}(\lambda_1, \lambda_2; \lambda_3, \lambda_4)$.

At tree-level the process is given by Higgs radiation off the b-quark line; see Fig. 1. The tree-level amplitude $\mathcal{A}_0(\lambda_1, \lambda_2; \lambda_3, \lambda_4)$ is therefore proportional to λ_{bbH} the

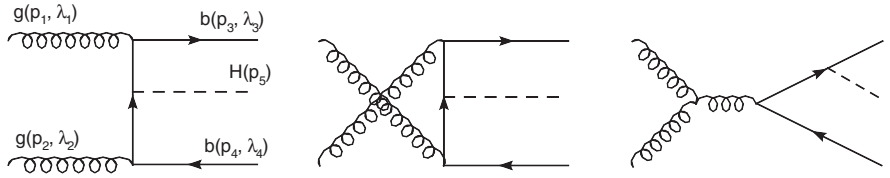

FIG. 1. All the eight Feynman diagrams can be obtained by inserting the Higgs line to all possible positions in the bottom line.

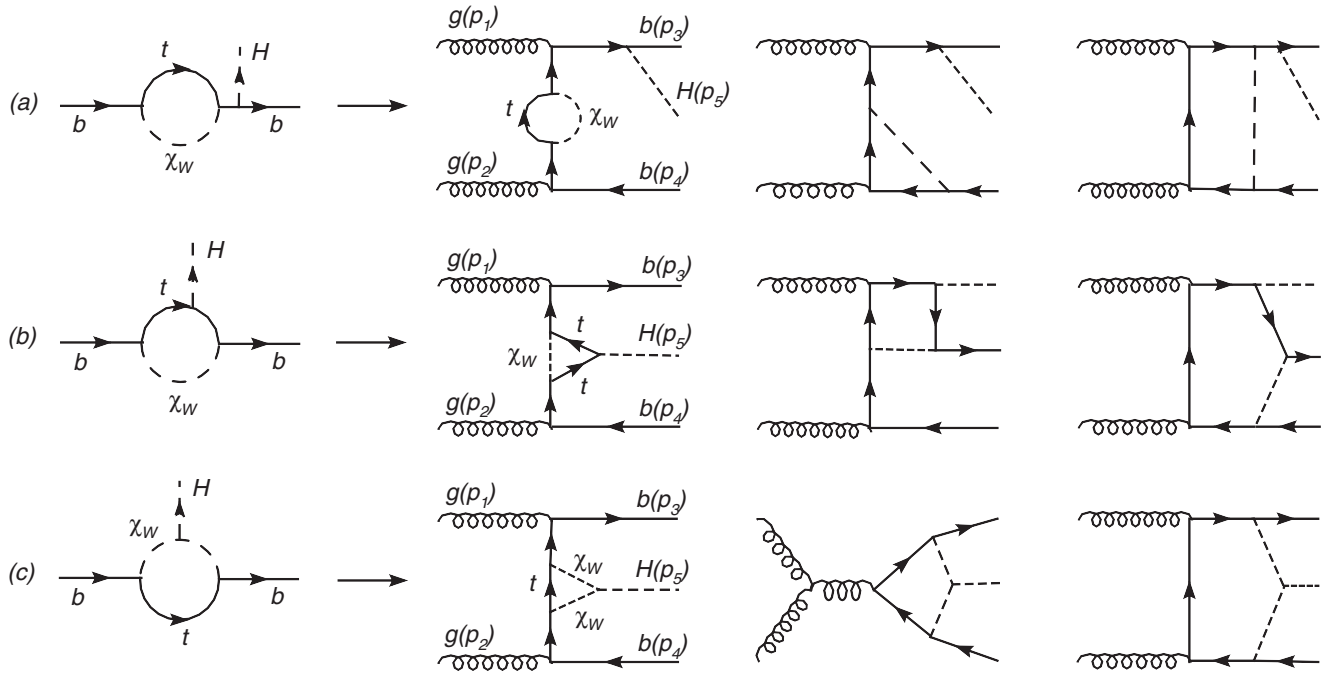

FIG. 2. All the diagrams in each group can be obtained by inserting the two gluon lines or one triple gluon vertex [shown in class (c)] to all possible positions in the generic bottom line, which is the first diagram on the left.

Higgs coupling to b. As has been done in previous analyses [4,14,15], for the exclusive $b\bar{b}H$ final state, we will require the outgoing b and $\bar{b}$ to have transverse momenta $|\mathbf{p}_T^{b,\bar{b}}| \geq 20$ GeV and pseudorapidity $|\eta^{b,\bar{b}}| < 2.5$. These kinematical cuts reduce the total rate of the signal but also greatly reduce the QCD background. As pointed in [16] these cuts also stabilize the scale dependence of the QCD NLO corrections compared to the case where no cut is applied. In the approximation of neglecting the bottom mass the whole contribution vanishes, since the Higgs coupling to b vanishes. The massless bottom limit can also be taken, but by keeping λ_{bbH} as an independent parameter with a nonzero value. In this limit the tree-level contribution consists of only the amplitude $\mathcal{A}_0(\lambda_1, \lambda_2; \lambda, -\lambda)$.[2] This turns out to be a very good approximation with the cuts we have taken; see [4].

[2]The helicity amplitude method and the convention we use in this paper for the definition of the helicity state are based on [4,17].

At the one-loop level the electroweak effects introduce a rich structure even in the limit where one takes the leading Yukawa (top and Higgs) couplings that are most easily given by the contribution of the top/charged Goldstones contribution in the Feynman gauge [4]; see Fig. 2. At one-loop, the diagrams are classified into three QCD gauge invariant classes as displayed in Fig. 2. The Higgs couples to the bottom quark in class (a), to the top quark in the class (b), and to the charged Goldstone boson in class (c). As shown in Fig. 2, each class can be efficiently reconstructed from the one-loop vertex $b\bar{b}H$, depending on which leg one attaches the Higgs, by then grafting the gluons in all possible ways. The difference in the coupling structure is another indication that each group forms a QCD gauge independent subset; see [4] for details. The analysis of [4] reveals that the contribution of class (a) at NLO is about -0.1% and thus can be totally neglected. Class (a) contribution naturally vanishes in the limit $\lambda_{bbH} = 0$ as does the tree-level. In this limit, the process is loop induced and triggered by diagrams in classes (b) and (c). Moreover in the limit $m_b \to 0$ with $\lambda_{bbH} \neq 0$, the one-loop corrections

induce new helicity structures compared to those found at tree-level in this limit.

When trying to extend the study we have performed in [4] for $M_H > 2M_W$ we encountered severe numerical instabilities for the cross section involving the square of the one-loop induced amplitude, which is the only remaining contribution in the limit $\lambda_{bbH} \to 0$. At the level of the NLO which involves the interference term between the tree-level and one-loop amplitudes no instability was present. On close inspection it was found that the instabilities were only due to the contribution from class (c), in particular, to the box diagrams, including the box obtained from the reduction of the pentagon diagrams as displayed in Fig. 4. At the partonic gluon-gluon level it was found there is no instability for $\sqrt{s_{gg}} < 2m_t$ and that independently of M_H and $\sqrt{s_{gg}}$ the result was completely stable for $m_t = M_W$. These threshold conditions were a sign for the possible existence of a leading Landau singularity for the box diagrams whose square is not integrable. The pentagon diagram in class (c) has no LLS but contains a subleading Landau singularity which is exactly the same as the LLS of the box diagram, obtained through the reduction of the pentagon to boxes. Some triangle diagrams of class (c) have also LLS (see Appendix C) but they are integrable hence do not cause any numerical instability. Since such singularities are little known nowadays and hardly encountered though we have referred to a few examples from the relatively recent literature in the introduction, we will discuss the issue of the LLS, their location and the condition on their appearance in the next section.

Before that, let us remind the reader that, to calculate the cross sections, we use the same helicity amplitude method as the one used and explained in [4]. Details of the renormalization scheme, for the NLO, and the optimization implemented in our code are the same as in [4]. To check the amplitudes and the cross sections we perform (QCD) gauge invariance tests and verify that our results are ultraviolet finite; see [4] for details of implementing these checks.

III. LANDAU SINGULARITIES

Part of the discussion in this section has been summarized in [11] and relies on [5,6] although a few results are new.

A. Conditions for a Landau singularity and the nature of the singularity

Consider the one-loop process $F_1(p_1) + F_2(p_2) + \ldots F_N(p_N) \to 0$, where F_i stands for either a scalar, fermion, or vector field with momentum p_i as in Fig. 3. The internal momentum for each propagator is q_i with $i = 1, \ldots N$. Each momentum q_i is associated with one real Feynman parameter x_i, respectively. The scalar N-point loop integral in D space-time dimension reads

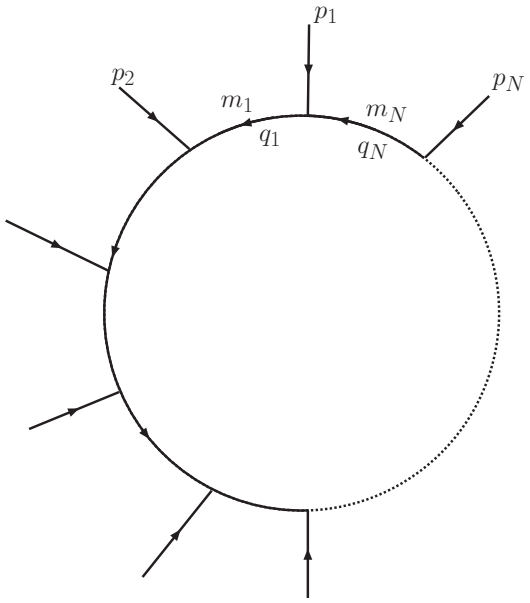

FIG. 3. One-loop Feynman diagram with N external particles.

$$\begin{aligned} T_0^N &\equiv \int \frac{d^D q}{(2\pi)^D i} \frac{1}{D_1 D_2 \cdots D_N}, \\ D_i &= q_i^2 - m_i^2 + i\varepsilon \quad \text{with} \quad \varepsilon > 0, \\ q_i &= q + r_i \quad \text{and} \quad q_i = q_i^*, \\ r_i &= \sum_{j=1}^{i} p_j, \qquad i = 1, \ldots, N; \end{aligned} \tag{1}$$

$q_i = q_i^*$ comes from the fact that the q-integration hypercontour is along the real axis, according to the (infinitesimal) $i\varepsilon$ prescription. The Feynman parameter representation reads

$$T_0^N = \Gamma(N) \int_0^\infty dx_1 \cdots dx_N \delta\Big(\sum_{i=1}^N x_i - 1\Big) \int \frac{d^D q}{(2\pi)^D i} \times \frac{1}{(x_1 D_1 + x_2 D_2 + \cdots x_N D_N)^N}. \tag{2}$$

Because of the Dirac delta function, the integration boundary in the Feynman parameter space is $x_i = 0$, $i = 1, \ldots, N$. Thus the only important condition on x_i is that they are real and *not negative*. The singularities are given by the Landau conditions [5,6,18]

$$\begin{cases} \forall\ i x_i (q_i^2 - m_i^2) = 0, \\ \sum_{i=1}^N x_i q_i = 0, \\ q_i = q_i^*. \end{cases} \tag{3}$$

If Eq. (3) has a solution $x_i > 0$ for every $i \in \{1, \ldots, N\}$, i.e. *all particles in the loop are simultaneously on shell*, then the integral T_0^N has a leading Landau singularity. If a solution exists but with some $x_i = 0$ while the other x_i's are positive, the Landau condition corresponds to a sub-

leading Landau singularity. To keep the analysis general let us therefore assume that Eq. (3) admits a solution with $x_i = 0$ for $i = M+1, \ldots, N$ with $1 \le M \le N$ and $x_i > 0$ for every $i \in \{1, \ldots, M\}$. Equation (3) would read

$$\begin{cases} x_i = 0 \quad \text{for } i = M+1, \ldots, N, \\ q_i^2 = m_i^2, x_i > 0 \quad \text{for } i = 1, \ldots, M, \\ \sum_{i=1}^{M} x_i q_i = 0. \end{cases} \tag{4}$$

For $M = N$ one has a leading singularity, otherwise if $M < N$ this is a subleading singularity. Multiplying the third equation in Eq. (4) by q_j leads to a system of M equations

$$\begin{cases} Q_{11}x_1 + Q_{12}x_2 + \cdots Q_{1M}x_M = 0, \\ Q_{21}x_1 + Q_{22}x_2 + \cdots Q_{2M}x_M = 0, \\ \vdots \\ Q_{M1}x_1 + Q_{M2}x_2 + \cdots Q_{MM}x_M = 0, \end{cases} \tag{5}$$

where the Q matrix is defined as

$$\begin{aligned} Q_{ij} &= 2q_i.q_j = m_i^2 + m_j^2 - (q_i - q_j)^2 \\ &= m_i^2 + m_j^2 - (r_i - r_j)^2; \\ i, j &\in \{1, 2, \ldots, M\}, \end{aligned} \tag{6}$$

and use is made of the on shell constraint, i.e. the second equation in (4). Note that in Eq. (5) $x_i > 0$.

The necessary conditions for the appearance of a Landau singularity can be summarized as follows

$$\begin{cases} \det(Q) = 0 \\ x_i > 0 \\ q_i^2 = m_i^2 \\ q_i = q_i^* \end{cases} \tag{7}$$

for $i = 1, \ldots, M$. The last condition, already encoded in Eq. (3), will prove to be useful, as we shall see.

It has been shown by Coleman and Norton [19] that if the matrix Q_{ij} has *only one* zero eigenvalue then these equations are necessary and sufficient conditions for the appearance of a singularity in the physical region.

If some internal (external) particles are massless like in the case of six photon scattering [8], then some Q_{ij} are zero, the above conditions can be easily checked. However, if the internal particles are massive then it is difficult to check the second condition in Eq. (7) explicitly, especially if M is large. In this case, we can rewrite the second condition as follows

$$x_j = \det(\hat{Q}_{jM})/\det(\hat{Q}_{MM}) > 0, \qquad j = 1, \ldots, M-1, \tag{8}$$

where $\hat{Q}_{ij}$ is obtained from Q by discarding row i and column j from Q and $\det(\hat{Q}_{jM}) = d[\det(Q)]/(2dQ_{jM})$, $\det(\hat{Q}_{MM}) = d[\det(Q)]/dQ_{MM}$. If $\det(\hat{Q}_{MM}) = 0$ then condition Eq. (8) becomes $\det(\hat{Q}_{jM}) = 0$ with $j = 1, \ldots, M-1$.

The condition of vanishing Landau determinant means that Q has at least one zero eigenvalue. In general, Q has N real eigenvalues $\lambda_1, \ldots, \lambda_N$. Consider the case where Q has *only one* (non degenerate) very small eigenvalue $\lambda_N \ll 1$, which is what is occurring in our present calculation for $gg \to b\bar{b}H$. To leading order

$$\lambda_N = \frac{a_0}{a_1}, \qquad a_1 = \lambda_1\lambda_2 \ldots \lambda_{N-1} \neq 0, \qquad a_0 = \det(Q). \tag{9}$$

With $V = \{x_1^0, x_2^0, \ldots, x_N^0\}$ the eigenvector corresponding to λ_N, we define $v^2 = V.V$. We will assume that $\lambda_i > 0$ for $i = 1, \ldots, K$ and $\lambda_j < 0$ for $j = K+1, \ldots, N-1$ with $0 \le K \le N-1$. It can then be shown that in D dimension (see Appendix A).

$$\begin{aligned} (T_0^N)_{\text{div}} &= \frac{1}{\pi}\frac{(-1)^{N+1}}{2^{(N+3)/2}}\frac{e^{i\pi\alpha_K}v}{\sqrt{(-1)^{2\alpha_K}a_1}}\frac{(4\pi)^{\alpha_D}\Gamma(\alpha_D)}{(\frac{1}{2}\lambda_N v^2 - i\varepsilon)^{\alpha_D}} \\ \alpha_K &= \frac{N-K+1}{2} \qquad \alpha_D = \frac{N-D+1}{2}. \end{aligned} \tag{10}$$

This result holds provided $a_1 \neq 0$ or in other words that the matrix Q does not have a degenerate zero eigenvalue. A similar result for the nature of the singularity has been derived in [18] in the general case of a multiloop diagram including the behavior of the nonleading singularity. The extraction of the overall, regular, factor which is the K-dependent part in Eq. (10) is more transparent in our derivation. As stressed earlier, the above result holds provided $a_1 \neq 0$. This general result has been derived with the assumption that formally $N - D + 1 > 0$, however unlike in [18] we can trivially analytically continue the result by using dimensional regularization with $D = 4 - 2\epsilon$ so that we can easily derive the nature of the singularity from Eq. (10) even for the case of $N \le 3$ in $D = 4$. For the box in 4 dimensions, $N = 4$, $D = 4$, $a_0 \to 0$, and $a_1 \neq 0$, we get

$$(T_0^4)_{\text{div}} = \frac{e^{i\pi(3-K)/2}}{4\sqrt{(-1)^{3-K}\det(Q_4)} - i\varepsilon}. \tag{11}$$

This shows that $(T_0^4)_{\text{div}}$ is integrable but its square is not. In the case $N = 3$ (the triangle), $D = 4$, one gets (see Appendix A for an alternative derivation not based on dimensional regularization but along the one followed in [18])

$$(T_0^3)_{\text{div}} = \frac{e^{i\pi(2-K)/2}v}{8\pi\sqrt{(-1)^{2-K}\lambda_1\lambda_2}}\ln(\lambda_3 v^2 - i\varepsilon). \tag{12}$$

T_0^3 and its square are therefore integrable.

The situation becomes more complicated when Q has a degenerate zero eigenvalue which happens in the case of the box diagram obtained in the case of the 6 photon amplitude or $gg \to W^+W^-$ [20] with massless internal

particles. In $D = 4$ and for $N \geq 6$ a leading Landau singularity does not obtain; see, for example, p. 115 of [6]. We leave some of these issues for another publication though and will concentrate here only on our process.

B. Application to $gg \to b\bar{b}H$

Having set the stage for the occurrence of the Landau singularities we now turn to check that the numerical instabilities found in $gg \to b\bar{b}H$ are indeed due to a Landau singularity. We concentrate on the box diagram in Fig. 4 which can contribute a leading Landau singularity. The leading singularity of the threepoint function relevant for our problem is studied in Appendix C and serves as good starting point for the discussion to follow. The associated five-point function where both external gluons attach to the internal top quark has no leading Landau singularity but rather a subleading Landau singularity which is exactly the same as the leading singularity that appears in the box diagram in Fig. 4. It is thus enough to study, in detail, the structure and the singularity behavior of this box diagram. We will keep the bottom quark massless unless otherwise stated.

Defining the invariants $s = s_{gg} = (p_1 + p_2)^2$, $s_1 = (p_3 + p_5)^2$, $s_2 = (p_4 + p_5)^2$, and the on shell conditions $p_1^2 = p_2^2 = p_3^2 = p_4^2 = 0$, $p_5^2 = M_H^2$, the kinematically allowed phase-space region leads to the constraint

$$M_H^2 \leq s_1 \leq s, \qquad M_H^2 \frac{s}{s_1} \leq s_2 \leq M_H^2 + s - s_1. \quad (13)$$

We need to keep these constraints in mind as the solution of the Landau equations may fall outside the phase space.

In terms of these invariants, the scalar box integral depicted in Fig. 4 writes, in the nomenclature of LOOPTOOLS, for example, as

$$T_0^4(s_1, s_2) = D_0(M_H^2, 0, s, 0, s_1, s_2, M_W^2, M_W^2, m_t^2, m_t^2). \quad (14)$$

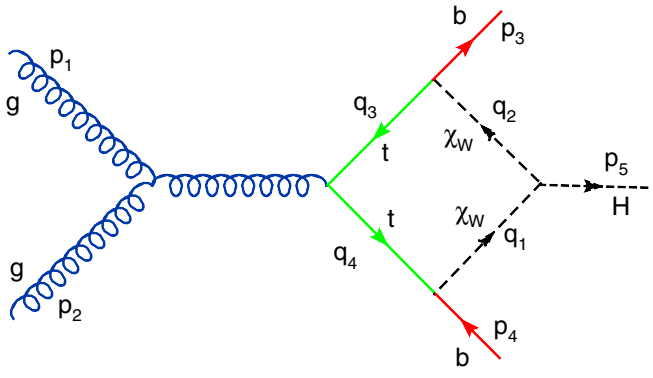

FIG. 4 (color online). A box diagram contributing to $gg \to b\bar{b}H$ that can develop a Landau singularity for $M_H \geq 2M_W$ and $\sqrt{s} \geq 2m_t$, i.e. all the four particles in the loop can be simultaneously on shell.

1. On shell and real conditions on the internal momenta q_i

For the leading Landau singularity of the box in Fig. 4, the on shell conditions on the internal particles read as $q_1^2 = q_2^2 = m_1^2 = m_2^2 = M_W^2$, $q_3^2 = q_4^2 = m_3^2 = m_4^2 = m_t^2$. The condition of real $q_i = (q_i^0, \mathbf{q}_i)$ means that $\mathbf{q}_i^2 \geq 0$. At each vertex, one has

$$\lambda(M_i^2, m_i^2, m_{i+1}^2) = (M_i^2 - (m_i + m_{i+1})^2) \times (M_i^2 - (m_i - m_{i+1})^2) \geq 0,$$
$$M_i^2 = (q_i - q_{i+1})^2, \quad (15)$$

with the usual λ kinematical function, vertex i is identified as the vertex to which the vector q_i points according to Fig. 4. M_i is the invariant mass of the external leg at vertex i. Applying the condition of Eq. (15) for the cases $i = 1, 3$ we get

$$M_H \geq 2M_W \quad \text{and} \quad \sqrt{s} \geq 2m_t. \quad (16)$$

This requires that the normal thresholds for top-quark production and Higgs decay into a W pair be opened.

Condition $\sum_{i=1}^N x_i q_i = 0$ in Eq. (3) in the case of the leading Landau singularity with $x_i > 0$ is nothing else but the addition of N vectors, $x_i q_i$, with norm $|x_i m_i|$. This says, for example, that not all time components q_i^0 can be positive or negative. For $N = 4$, either one vector has $\text{sign}(x_i q_i^0)$ opposite to all the other three or there are 2 vectors $x_i q_i^0$ with positive signs while the others have a negative sign. In our case, it is easy to see that we can only take $q_{1,4}^0 > 0$, $q_{2,3}^0 < 0$. These simple considerations furnish additional inequalities that are constraints on the appearance of a LLS. Applied at the four vertices, for example, in the rest frame of one of the internal on shell particle [21], these give the additional normal thresholds of this four-point function

$$m_t > M_W, \quad (17)$$

$$s_1 \geq (m_t + M_W)^2 \quad \text{and} \quad s_2 \geq (m_t + M_W)^2. \quad (18)$$

These strong requirements on the opening up of the normal thresholds will delimit the region where a LLS will occur, as given by the vanishing of the Landau determinant. These normal thresholds are also normal thresholds of the reduced diagrams, three-point, and two-point functions, obtained from $x_i = 0$ and are necessary condition for a LLS for these integrals; see Appendix C.

The on shell and real conditions on the internal momenta q_i with $\sum x_i q_i = 0$, $x_i > 0$ have been given a beautiful pictorial physical interpretation by Coleman and Norton [19]. Each q_i can be regarded as the physical momentum of a physical particle; we can associate to the Feynman diagram a space-time graph of a process with on shell classical particles moving forward in time; and $x_i m_i$ can be regarded as the proper time of particle i. The vertices are

regarded as space-time points. $\Delta X_i = x_i q_i$ (no sum over i) is a space-time separation.

2. Landau determinant

The necessary conditions given by the inequalities above having to do with the opening up of normal thresholds need to be supplemented by the requirements of a vanishing Landau determinant. The reduced matrix, $S^{(4)}$, which is equivalent in this case to the Q matrix for studying the Landau singularity, is given by

$$S_4 = \begin{pmatrix} 1 & \frac{2M_W^2 - M_H^2}{2M_W^2} & \frac{m_t^2 + M_W^2 - s_1}{2M_W m_t} & \frac{M_W^2 + m_t^2}{2M_W m_t} \\ \frac{2M_W^2 - M_H^2}{2M_W^2} & 1 & \frac{M_W^2 + m_t^2}{2M_W m_t} & \frac{m_t^2 + M_W^2 - s_2}{2M_W m_t} \\ \frac{m_t^2 + M_W^2 - s_1}{2M_W m_t} & \frac{M_W^2 + m_t^2}{2M_W m_t} & 1 & \frac{2m_t^2 - s}{2m_t^2} \\ \frac{M_W^2 + m_t^2}{2M_W m_t} & \frac{m_t^2 + M_W^2 - s_2}{2M_W m_t} & \frac{2m_t^2 - s}{2m_t^2} & 1 \end{pmatrix},$$

$$S_4^{ij} = \frac{Q_4^{ij}}{2m_i m_j}. \tag{19}$$

With s and M_H fixed one can study the behavior of the determinant as a function of the invariant s_1 and s_2. The determinant is a polynomial of order 2 in each of these variables. In terms of s_2, for example, it reads

$$\begin{aligned} \det(Q_4) &= 16 M_W^4 m_t^4 \det(S_4) = a s_2^2 + b s_2 + c \\ &= a\{(s_2 - s_2^0)^2 + \bar{\Delta}(s_1)\}, \\ a &= \lambda(s_1, m_t^2, M_W^2) = [s_1 - (m_t + M_W)^2] \\ &\quad \times [s_1 - (m_t - M_W)^2], \\ b &= 2\{-s_1^2(m_t^2 + M_W^2) + s_1[(m_t^2 + M_W^2)^2 \\ &\quad - (s - 2m_t^2)(M_H^2 - 2M_W^2)] + s M_H^2 (m_t^2 + M_W^2)\}, \\ s_2^0 &= -b/2a, \\ c &= s_1^2 (m_t^2 - M_W^2)^2 + 2M_H^2 s (m_t^2 + M_W^2) s_1 \\ &\quad + s M_H^2 [(s - 4m_t^2)(M_H^2 - 4M_W^2) \\ &\quad - 4(m_t^2 + M_W^2)^2], \\ \bar{\Delta}(s_1) &= -\frac{b^2 - 4ac}{4a^2}. \end{aligned} \tag{20}$$

Writing $\det Q_4$ as perfect square in s_2, like above, for example, and a remainder which is the discriminant of the quadratic form that does not depend on s_2 can be revealing. In our case, we find

$$\begin{aligned} \det(Q_4) = &- \det Q_2(s_1; m_t^2, M_W^2)\Bigg((s_2 - s_2^0)^2 \\ &- \frac{\det Q_3(s_1, M_H^2, 0; m_t^2, M_W^2, M_W^2)}{\det Q_2(s_1; m_t^2, M_W^2)} \\ &\times \frac{\det Q_3(s_1, s, 0; M_W^2, m_t^2, m_t^2)}{\det Q_2(s_1; m_t^2, M_W^2)}\Bigg). \end{aligned} \tag{21}$$

$\det Q_3$'s are the Landau determinants of the three-point function subdiagrams obtained from the original four-point function by shrinking one internal line to a point, forming subdiagrams where the invariant s_1 is an argument of these three-point functions. Likewise for $\det Q_2$ obtained by further shrinking one of the triangles. The corresponding two- and three-point functions are shown in Fig. 5. Our convention for $\det Q_{3,2}$ as concerns its arguments is given in Appendix C. The factorization in Eq. (21) can be derived [22] for symmetric matrices based on the Jacobi ratio theorem for determinants [23]. Each subdeterminant of the reduced three-point function can be further reduced into exactly such a factorized form; see Appendix C. This makes the identification of the subleading singularities very transparent. For example, $\det Q_2(s_1; m_t, M_W) = 0$ corresponds to a normal threshold; see Eq. (18). It occurs for $\sqrt{s_1} = m_t + M_W$ ($\sqrt{s_1} = m_t - M_W$ is outside the physical region for Higgs masses of interest). Obviously we could have written the quadratic form in any of the variables s_1, s_2, M_H^2, s, the completion of the determinant will be the product of the determinant of two subdiagrams.

3. Numerical investigation of the four-point function and the Landau determinant

We will always take $m_t = 174$ GeV and $M_W = 80.3766$ GeV. Our investigation starts by taking $\sqrt{s} = 353$ GeV, $M_H = 165$ GeV. The behavior of the Landau determinant, the real and imaginary parts of the four-point function T_0^4 are displayed in Fig. 6 as a function of s_1, s_2 within the phase space. We clearly see that the Landau determinant vanishes inside the phase space and leads to

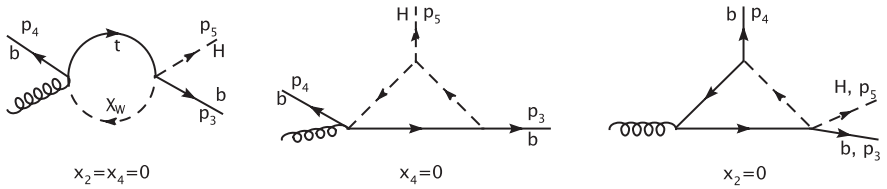

FIG. 5. Three reduced diagrams of the box diagram in Fig. 4, that contain s_1 as an invariant of the two- and three-point functions and whose Landau determinants are given in Eq. (21). The self-energy diagram has a normal threshold. The two triangle diagrams contain anomalous thresholds. Note that the singularity structure of the second diagram, in the s_1, M_H variables, is the same as the triangle studied in much detail in Appendix C but with $s_1 \to s_2$; see Fig. 19. The singularities of the second triangle can be obtained from the first one by $s \leftrightarrow M_H^2$, $m_t \leftrightarrow M_W$.

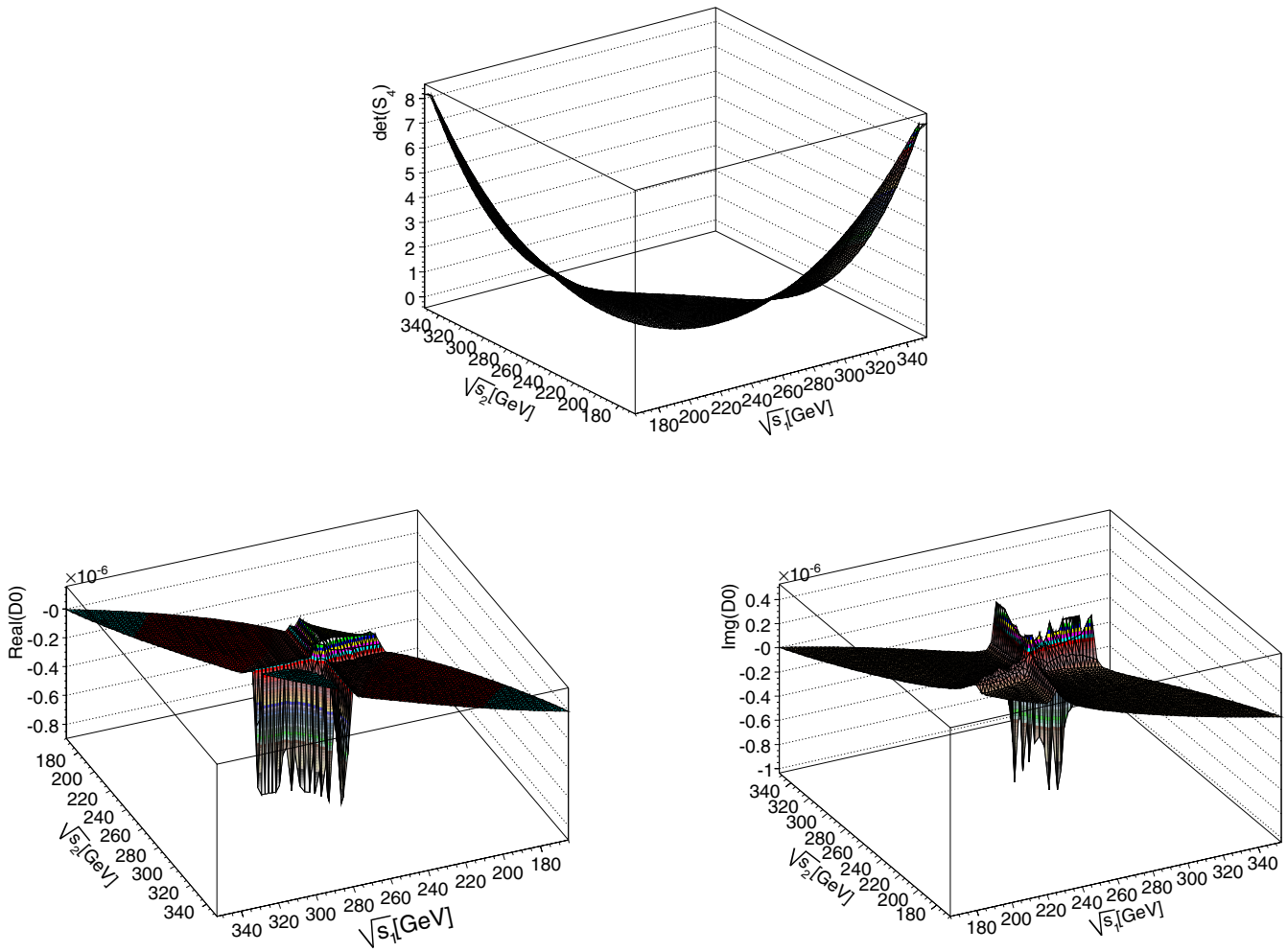

FIG. 6 (color online). The Landau determinant as a function of s_1 and s_2 (upper figure). The real and imaginary parts of D_0 as a function of s_1 and s_2. The figure for the real part of D_0 has been rotated since the structure is best seen with this view.

regions of severe instability in both the real and imaginary parts of the scalar integral.

To investigate the structure of the singularities in more detail let us fix $\sqrt{s_1} = \sqrt{2(m_t^2 + M_W^2)} \approx 271.06$ GeV, such that the properties are studied for the single variable s_2. This will also exhibit the subleading Landau singularities related to the reduced diagrams. In the variables s_2, these are exactly the same as the ones we uncovered through Eq. (21). They are represented in Fig. 5 allowing for $s_1 \rightarrow s_2$ (and $x_2 \rightarrow x_1$, $x_4 \rightarrow x_3$).

Figure 7 is very educative. We see that there are four discontinuities in the function representing the real part of the scalar integral in the variable $\sqrt{s_2}$.

(i) As s_2 increases, we first encounter a discontinuity at the normal threshold $\sqrt{s_2} = \sqrt{s_2^{\mathrm{tW}}} = m_t + M_W = 254.38$ GeV, representing $Hb \rightarrow Wt$. This corresponds to the solution (for the Feynman parameters) $x_{1,3} = 0$ and $x_{2,4} > 0$ of the Landau equations and can be associated to a leading Landau singularity for the two-point scalar integral.

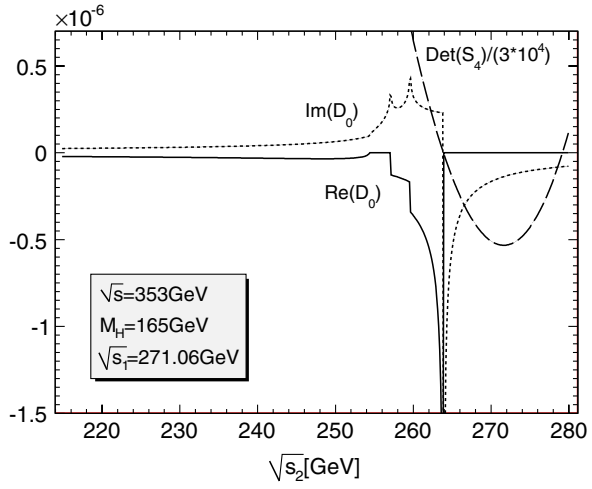

FIG. 7 (color online). The imaginary, real parts of D_0 and the Landau determinant as functions of $\sqrt{s_2}$.

(ii) The second discontinuity occurs $\sqrt{s_2} = 257.09$ GeV. This corresponds to an anomalous threshold of a reduced triangle diagram. This corresponds to the solution $x_3 = 0$ and $x_{1,2,4} > 0$ of the Landau equations (see Fig. 5). The singularity structure of this diagram is studied in more detail in Appendix C. We can explicitly check that $\sqrt{s_2} = 257.09$ GeV corresponds to the condition of vanishing determinant. One solution of this equation does not satisfy the sign condition Eq. (8), and is not even inside of phase space. As shown in Appendix C only one solution [see also Eq. (C11)] is acceptable with

$$\begin{aligned} s_2^H &= \frac{1}{2M_W^2}(M_H^2(M_W^2 + m_t^2) \\ &\quad - (m_t^2 - M_W^2)M_H\sqrt{M_H^2 - 4M_W^2}) \\ &= 2(m_t^2 + M_W^2) + (M_H^2 - 4M_W^2) \\ &\quad \times \left(1 + \frac{m_t^2 - M_W^2}{2M_W^2}\left(1 - \frac{1}{\sqrt{1 - 4M_W^2/M_H^2}}\right)\right), \end{aligned} \tag{22}$$

which gives $\sqrt{s_2^H} = 257.09$ GeV. Note that one of the necessary conditions for this anomalous threshold to occur in the physical region is $M_H \geq 2M_W$. At this *normal* threshold the value of s_2^H is $s_2^H = 2(m_t^2 + M_W^2)$; see Eq. (22).

(iii) The third discontinuity at $\sqrt{s_2} = 259.58$ GeV corresponds to the anomalous threshold of the reduced three-point function obtained from the box diagram by contracting to a point the x_1 line (see the third diagram in Fig. 5) so that $\det Q_3(s_1, s, 0; M_W^2, m_t^2, m_t^2) = 0$. Analogously $\sqrt{s_2} = 259.58$ GeV is given by

$$\begin{aligned} s_2^s &= \frac{1}{2m_t^2}(s(m_t^2 + M_W^2) - \sqrt{s}\sqrt{s - 4m_t^2}(m_t^2 - M_W^2)) \\ &= 2(m_t^2 + M_W^2) + (s - 4m_t^2) \\ &\quad \times \left(1 + \frac{m_t^2 - M_W^2}{2m_t^2}\left(1 - \frac{1}{\sqrt{1 - 4m_t^2/s}}\right)\right). \end{aligned} \tag{23}$$

(iv) The last singular discontinuity is the leading Landau singularity. The condition $\det(S_4) = 0$ for the box has two solutions which numerically correspond to $\sqrt{s_2} = 263.88$ GeV or $\sqrt{s_2} = 279.18$ GeV. Both values are inside the phase space; see Fig. 7. However after inspection of the corresponding sign condition, only $\sqrt{s_2} = 263.88$ GeV (with $x_1 \approx 0.53$, $x_2 \approx 0.75$, $x_3 \approx 0.77$) qualifies as a leading Landau singularity. $\sqrt{s_2} = 279.18$ GeV has $x_1 \approx -0.74$, $x_2 \approx -0.75$, $x_3 \approx 1.07$ and is outside the physical region.

The nature of the LLS in Fig. 7 can be extracted by using the general formula (11). With the input parameters given above, the Landau matrix has only one positive eigenvalue at the leading singular point, i.e. $K = 1$. The leading singularity behaves as[3]

$$D_0^{\text{div}} = -\frac{1}{16M_W^2 m_t^2\sqrt{\det(S_4) - i\varepsilon}}. \tag{24}$$

When approaching the singularity from the left, $\det(S_4) > 0$, the real part turns singular. When we cross the leading singularity from the right, $\det(S_4) < 0$, the imaginary part of the singularity switches on, while the real part vanishes. In this example, both the real and imaginary parts are singular because $\det(S_4)$ changes sign when the leading singular point is crossed.

4. The leading Landau singularity region in the $(M_H, \sqrt{s})$ *plane*

In practice, we will have to integrate over the s_1 and s_2 variables to obtain the total cross section at the partonic level. We will also have to integrate over $s = s_{gg}$ to arrive at the cross section at the pp level. Moreover, we would like to study the behavior of the cross section by varying M_H. It is therefore important to quickly localize the range or region in the $(\sqrt{s}, M_H)$ plane where the leading Landau singularity occurs. This approach should in fact be followed in more general cases to check if one might encounter a potential problem prior to carrying the full phase-space integration procedure with the full matrix elements. Necessary (but not sufficient) conditions on M_H and $\sqrt{s}$ to have a LLS correspond to the opening of normal thresholds as given in Eq. (16). These are easy to guess and are contained in the last two equations of Eq. (7). We have, however, to solve all of Eq. (7) together with the constraint that one is inside the phase space Eq. (13). This, in general, is too complicated to be done analytically in a situation like ours with four variables (M_H, s, s_1, s_2) and two parameters (M_W, m_t). However numerically the algorithm that goes through all the conditions is quite simple to implement. For instance, one can start with the Landau determinant written as a quadratic form in s_2 by first computing the discriminant of the quadratic equation and check whether the latter is positive or negative, assuming the solutions are in the physical region. If the discriminant is positive one checks if the corresponding solution does not conflict with the positivity solution as implemented in Eq. (8). If this condition is satisfied then there is a LLS. In our case, the result is shown in Fig. 8. We conclude that the LLS occurs when $2M_W \leq M_H < 211$ GeV and $2m_t \leq \sqrt{s} < 457$ GeV. The range of the LLS region depends on M_W and m_t. If $m_t/M_W \leq 1$ then the first two conditions in Eq. (7) can

[3]The singularity of the three-point function is logarithmic; see Eq. (12). Figure 7 shows 2 three-point singularities which look as if better behaved within LOOPTOOLS.

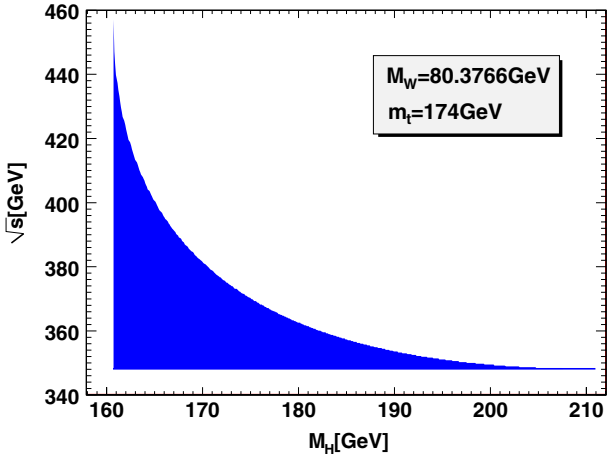

FIG. 8 (color online). The region of the leading Landau singularity in the variables $\sqrt{s} = \sqrt{s_{gg}}, M_H$.

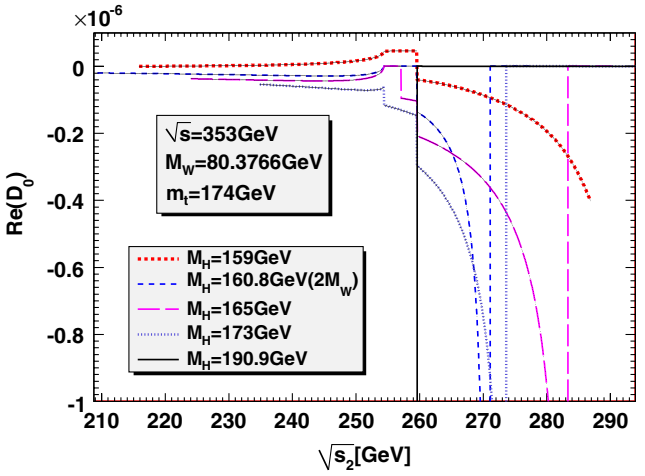

FIG. 9 (color online). The real part of D_0 as a function of $\sqrt{s_2}$ for various values of M_H. For $M_H = 2M_W$, we have taken $s_1 = 2(m_t^2 + M_W^2)$. For the other cases, we take $s_1 = 260$ GeV.

never be satisfied. In particular, if $m_t/M_W = 1$ then the Landau determinant can vanish but the sign condition cannot be realized. When $M_H > 210$ GeV or $\sqrt{s} > 456$ GeV the Landau determinant $\det(Q_4)$ can vanish inside the phase space but the sign condition $x_i > 0$ cannot be fulfilled.

The region of the leading Landau singularity in Fig. 8 is a surface of singularities in the plane of the kinematical variables $\sqrt{s} = \sqrt{s_{gg}}, M_H$. This is bounded by three curves. It is important to stress again that the horizontal and vertical lines or boundaries correspond to the normal thresholds. These lines are also *tangent* to the upper curve delimiting the surface of LLS. We will get back to this property later.

The algorithm we have just outlined is very easy to implement. The importance of the sign condition is crucial in determining the boundary of the leading Landau singularity region which occurs when $x_i \to 0$. We will come back to this point shortly. Before doing so, it is worth coming back to the behavior of D_0 as a function of s_2 (like what we have shown in Fig. 7) and see how the location of the leading Landau singularity and the other discontinuities (related to other thresholds) move as M_H is varied.

As in Fig. 7, we fix $\sqrt{s} = 353$ GeV and $\sqrt{s_1}$ but with $\sqrt{s_1} = 260$ GeV for $M_H = 159, 165, 190$ GeV. All the curves will therefore show the two-point function discontinuity (normal threshold) at $\sqrt{s_2^{\mathrm{tW}}} = 254.38$ GeV and the three-point function discontinuity at $\sqrt{s_2^s} = 259.58$ GeV; see Eq. (23). The other three-point function discontinuity at $\sqrt{s_2^H}$ and the leading Landau singularity, if at all there, will of course move. The results are shown in Fig. 9.

(i) For $M_H = 159$ GeV only the normal threshold at $\sqrt{s_2^{\mathrm{tW}}}$, and the $\sqrt{s_2^s}$ discontinuity show up as expected since $M_H < 2M_W$.

(ii) For $M_H = 165$ GeV ($M_H > 2M_W$), the other three-point singularity shows at $\sqrt{s_2^H} = 257.09$ GeV, together with the LLS at $\sqrt{s_2^{\mathrm{LLS}}} \approx 283.5$ GeV. As $\sqrt{s_1}$ is increased the LLS moves to smaller values of s_2, closer to the three-point function singularity as can be seen by comparing with Fig. 7 for the same value of M_H but higher value of $\sqrt{s_1}$. This will be a common feature with the other cases with $M_H > 2M_W$, until the LLS disappears from the physical region. For $\sqrt{s_1} < 260$ GeV, no LLS develops. We have the ordering $\sqrt{s_2^{\mathrm{tW}}} < \sqrt{s_2^H} < \sqrt{s_2^s} < \sqrt{s_2^{\mathrm{LLS}}}$.

(iii) For $M_H \approx 173$ GeV, $\sqrt{s_2^H} = \sqrt{s_2^{\mathrm{tW}}} = 254.38$ GeV, i.e the s_2^H threshold coincides with the normal threshold. The LLS starts showing up at $\sqrt{s_2} \approx 274$ GeV when $\sqrt{s_1} = 260$ GeV and moves to smaller values of s_2 as $\sqrt{s_1}$ increases. We have the ordering $\sqrt{s_2^{\mathrm{tW}}} = \sqrt{s_2^H} < \sqrt{s_2^s} < \sqrt{s_2^{\mathrm{LLS}}}$. The coincidence $\sqrt{s_2^{\mathrm{tW}}} = \sqrt{s_2^H}$ signals the termination a leading singularity in the three-point function; see Appendix C. As we increase M_H, the LLS moves to smaller values of s_2 and the s_2^H discontinuity disappears from the physical region.

(iv) For the special value $M_H = 190.88$ GeV, the s_2^H singularity has moved out of the physical region but now the LLS coincides with the location of the s_2^s three-point function singularity. We therefore have $\sqrt{s_2^{\mathrm{tW}}} < \sqrt{s_2^s} = \sqrt{s_2^{\mathrm{LLS}}}$. For $M_H > 190.88$ GeV the LLS disappears from the physical region.

(v) Finally, we consider the special case of the threshold $M_H = 2M_W$ where $\sqrt{s_2^H} = 271.06$ GeV. One has to change s_1 in the range defined by Eq. (13) with the

condition $s_1 \geq (m_t + M_W)^2$ to make the LLS appear. It is easy to find out that the LLS only occurs when $\sqrt{s_1} = \sqrt{2(m_t^2 + M_W^2)} = 271.06$ GeV and the LLS position coincides with the position of the three-point singularity $\sqrt{s_2^H}$. We have the ordering $\sqrt{s_2^{\mathrm{tW}}} < \sqrt{s_2^s} < \sqrt{s_2^H} = \sqrt{s_2^{\mathrm{LLS}}}$.

For future reference, it is worth noting that the LLS region opens up rather sharply when the normal thresholds open up and the bulk of the region is concentrated around these thresholds. Already for $M_H \geq 200$ GeV the region squeezes into a very thin line.

5. The leading Landau singularity region: analytical insight

We will take two approaches. The first one is based on the observation that the boundary of the singularity region corresponds to a coincidence of a leading Landau singularity with a subleading singularity, this is the termination of the LLS [21,22,24]. The second approach starts directly from the constraint or equation given by the vanishing of the Landau determinant. The extrema of this equation with respect to a particular choice of kinematical variables will define the termination of the LLS. Interpreting the equation as that defining a surface or a hypercurve, the extrema are tangents to the surface and are parallel to the corresponding coordinate variables. This will become clearer when we expose the derivation.

(i) A study of the LLS in the three-point scalar integral relevant to our problem is quite simple since this function does, for fixed m_t, M_W, involve a very small number of variables. Yet the study (see Appendix C) reveals some very general features. There is an LLS region, or curve, that is bounded by the normal threshold. This a manifestation of the fact that at the boundary, the leading singularity moves to the subleading singularity [21,22,24]. This is also a phenomenon we observed in Sec. III B 4. Let us now analytically derive the surface shown in Fig. 8, or rather the curve representing its boundaries in the (M_H, s) range. The lower bounds are just given by the normal thresholds of the two-point function so that $M_H \geq 2M_W$ and $\sqrt{s} \geq 2m_t$; see Eq. (16). For each value of (M_H, s) there is a curve of LLSs defined by $\mathcal{F}(s_1, s_2, |M_H, s)$ which is constrained by the vanishing of $\det Q_4(s_1, s_2)$ and subject to the sign conditions. For this discussion about the (M_H, s) range it is sufficient to only keep the (s_1, s_2) dependence of $\det Q_4$. As we scan over (M_H, s) we span a surface of LLSs. The key observation is that the curves terminate at a point corresponding to a subleading singularity, in this case a leading singularity of one of the three-point function subdiagrams which itself will terminate at the two-point singularity, i.e. the normal threshold. For instance, writing $\det(Q_4)$ as a quadratic polynomial of s_2 as we did in Eq. (21), there are 2 three-point sub-LLSs given by each $\det Q_3$ in Eq. (21) vanishing. The solutions of the latter are given, respectively, by Eq. (22) and (23). Let us take for definiteness the subleading singularity corresponding to s_2^H in Eq. (22). The argument works just as well with the other three-point singularity s_2^s. The coincidence constraint implies, for s_2, for example, a solution $\hat{s}_2 = s_2 = s_2^H$ and $\det Q_4(s_1, s_2) = 0$ (with the proviso about the sign condition). Exactly the same argument can be put but now solving for the variable s_1 and exploiting the fact that our problem is symmetric in $s_1 \leftrightarrow s_2$. The coincidence problem or the constraint we are looking for translates into

$$\begin{aligned} &s_2 = s_2^H \quad \text{and} \quad \det Q_4(s_1, s_2) = 0, \\ &s_1 = s_2^H \quad \text{and} \quad \det Q_4(s_1, s_2) = 0, \\ &\Rightarrow \det Q_4(\hat{s}_2, \hat{s}_2) = 0 \quad \text{and} \quad \hat{s}_2 = s_2^H. \end{aligned} \tag{25}$$

Only one solution to $\det Q_4(\hat{s}_2, \hat{s}_2) = 0$ passes the LLS sign conditions, with

$$\hat{s}_2 = 2(m_t^2 + M_W^2) - \sqrt{(s - 4m_t^2)(M_H^2 - 4M_W^2)}. \tag{26}$$

Equating Eq. (26) with Eq. (22), we arrive at the equation of the termination curve

$$\begin{aligned} \sqrt{(s - 4m_t^2)} = \frac{1}{2M_W^2}(M_H(m_t^2 - M_W^2) \\ - (m_t^2 + M_W^2)\sqrt{(M_H^2 - 4M_W^2)}). \end{aligned} \tag{27}$$

Observe that this equation shows, in a very transparent way, that all thresholds:

$$m_t > M_W, \qquad M_H \geq 2M_W, \qquad \sqrt{s} \geq 2m_t$$

need to be open simultaneously. We can invert Eq. (27) to write the solution in terms of M_H. To arrive at the same result, it is more judicious however to go through exactly the same steps but choosing s_2^s instead of s_2^H. We derive

$$\begin{aligned} \sqrt{(M_H^2 - 4M_W^2)} = \frac{1}{2m_t^2}(\sqrt{s}(m_t^2 - M_W^2) \\ - (m_t^2 + M_W^2)\sqrt{(s - 4m_t^2)}). \end{aligned} \tag{28}$$

The maximum value of M_H $(\sqrt{s})$ is obtained by setting $\sqrt{s} = 2m_t$ $(M_H = 2M_W)$, i.e. when the LLS, the 2 three-point sub-LLSs and the normal threshold coincide. We have

$$\begin{aligned} 4M_W^2 \leq M_H^2 \leq 4M_W^2 + \frac{(m_t^2 - M_W^2)^2}{m_t^2}, \\ 4m_t^2 \leq s \leq 4m_t^2 + \frac{(m_t^2 - M_W^2)^2}{M_W^2}. \end{aligned} \tag{29}$$

or numerically,

$$\begin{aligned} 348.00 \text{ GeV} \leq \sqrt{s} \leq 457.05 \text{ GeV} \quad \text{and} \\ 160.75 \text{ GeV} \leq M_H \leq 211.13 \text{ GeV}. \end{aligned} \tag{30}$$

Of course, these analytical formulae reproduce exactly the curve in Fig. 8 that was obtained numerically. For example, we have arrived at the same, unique solution by taking $s_{1,2} = s_2^H$ and $s_{1,2} = s_2^s$ in turn. This also means that the curve is also given by

$$s_2^s = s_2^H. \tag{31}$$

This constraint gives directly the equation for the bounding curve and avoids having to solve for s_1 or s_2 as is done as an intermediate step in Eq. (26).

(ii) Another interesting interpretation of the bounding curve which also leads to Eq. (31) is based on the following. The leading Landau singularity in the (s_1, s_2) plane is a solution of $\det Q_4(s_1, s_2) = 0$ supplemented by the sign conditions. With fixed values of the internal masses, the constraint $\det Q_4(s_1, s_2, s, M_H^2) = 0$ is a constraint on the kinematical invariants for which a LLS can occur. This therefore defines a surface of LLS singularities, which one may want to visualize in the plane (s_1, s_2) or (s, M_H^2). Within the plane (s_1, s_2), the extrema of this surface are given by the tangents to this surface which are parallel to the coordinate variables, in this case s_1, s_2 [22], therefore

$$\begin{aligned} &\frac{\partial \det Q_4(s_1, s_2)}{\partial s_2} = 0 \quad \text{with} \quad \det Q_4(s_1, s_2) = 0 \quad \text{and} \\ &\frac{\partial \det Q_4(s_1, s_2)}{\partial s_1} = 0 \quad \text{with} \quad \det Q_4(s_1, s_2) = 0. \end{aligned} \tag{32}$$

These conditions are best exploited by using the quadratic form of $\det Q_4(s_1, s_2)$ in s_2 (and s_1) given in Eq. (21). The first equation in Eq. (32) with the help of Eq. (21) leads to

$$\det Q_3(s_1, M_H^2) \det Q_3(s_1, s) = 0. \tag{33}$$

The second equation, using again the same quadratic form in Eq. (21) leads to

$$\begin{aligned} &\frac{\partial \det Q_3(s_1, M_H^2)}{\partial s_1} \det Q_3(s_1, s) \\ &\quad + \frac{\partial \det Q_3(s_1, s)}{\partial s_1} \det Q_3(s_1, M_H^2) = 0. \end{aligned} \tag{34}$$

Equations (33) and (34) have three solutions. The first solution requires (a) *both* subdeterminants in Eq. (21) to vanish, $\det Q_3(s_1, M_H^2) = \det Q_3(s_1, s) = 0$. This requirement is exactly the condition given in Eq. (27). The other solutions of Eqs. (33) and (34) give the boundaries related to the *normal thresholds*, (b) $\det Q_3(s_1, M_H^2) = \frac{\partial \det Q_3(s_1, M_H^2)}{\partial s_1} = 0$ which implies [see Eq. (C14)] the normal threshold $M_H = 2M_W$ is reached, while the third solution (c) $\det Q_3(s_1, s) = \frac{\partial \det Q_3(s_1, s)}{\partial s_1} = 0$ corresponds to the normal threshold $s = (2m_t)^2$. These equations for the boundary define the LLS region presented in Fig. 8. Note that (b) and (c) can also be derived from (a) if one insists on finding the extrema of the curve $\det Q_3(s_1, M_H^2) = 0$ for example. This is the same argument that is used in Appendix C for the three-point function. Here we can carry this argument one step further starting from the fact that $\det Q_3 = 0$ is a condition for the Landau singularity of a three-point function. The extrema and tangent argument applied at this level will show that the range in M_H and s are given by the vanishing of the corresponding $\det Q_2$ which give the normal thresholds, $M_H = 2M_W$ and $s = (2m_t)^2$. This derivation shows that when the normal threshold is met all singularities of the two-, three- and four-point function coalesce. Observe that in Fig. 8 the lines given by $M_H = 2M_W$ and $\sqrt{s} = 2m_t$ are not only boundaries of the LLS region but also tangents to the extremum bounding curve given by Eq. (27).

The arguments given above can be applied to derive the bounding curve and the range of the LLSs in the (s_1, s_2) plane after elimination of the variables (M_H^2, s) and taking into account the normal threshold condition, $s_{1,2} > (m_t + M_W)^2$ as the lower bound. The starting point in this case is to express $\det Q_4$ as a quadratic polynomial in M_H^2, for example. The solution of the bounding curve is given by

$$\begin{aligned} s_1 - s_2 = \frac{m_t^2 - M_W^2}{m_t^2 + M_W^2} &\left(\sqrt{\lambda(s_1, m_t^2, M_W^2)}\right. \\ &\left. - \sqrt{\lambda(s_2, m_t^2, M_W^2)}\right). \end{aligned} \tag{35}$$

This translates into the bounds

$$\begin{aligned} &(m_t + M_W)^2 \le s_{1,2} \le (m_t + M_W)^2 + \frac{(m_t^2 - M_W^2)^2}{m_t M_W}, \\ &\text{numerically} \qquad 254.38\ \text{GeV} \le \sqrt{s_{1,2}} \le 324.44\ \text{GeV}. \end{aligned} \tag{36}$$

IV. THE WIDTH AS A REGULATOR OF THE LANDAU SINGULARITY

As we have seen the leading Landau singularity requires all internal particles to be on their mass shell; see, for example, Eq. (7). This is akin to the usual singularity that occurs on resonance for a massive particle. These equations also show that if any parameter m_i is complex with a nonzero imaginary part, the singularity is avoided. For an unstable particle the width provides this imaginary part. As can be inferred from Eq. (7), mathematically, the width effect is to move the Landau singularities into the complex plane, so they do not occur in the physical region (the real axis). For our problem, the Landau condition in the interpretation of Coleman and Norton through Eq. (17), $m_t > M_W$, clearly shows that the singularity develops because of the instability of the top quark. Therefore, in principle, one should only include the width of the top as a regulator. Including the width of an unstable particle, whereby the mass of the internal particle becomes complex effectively sums a subset of higher order Feynman diagrams thereby taming the Landau singularity [10]. On the other hand, if one goes to higher order to implement the width then we

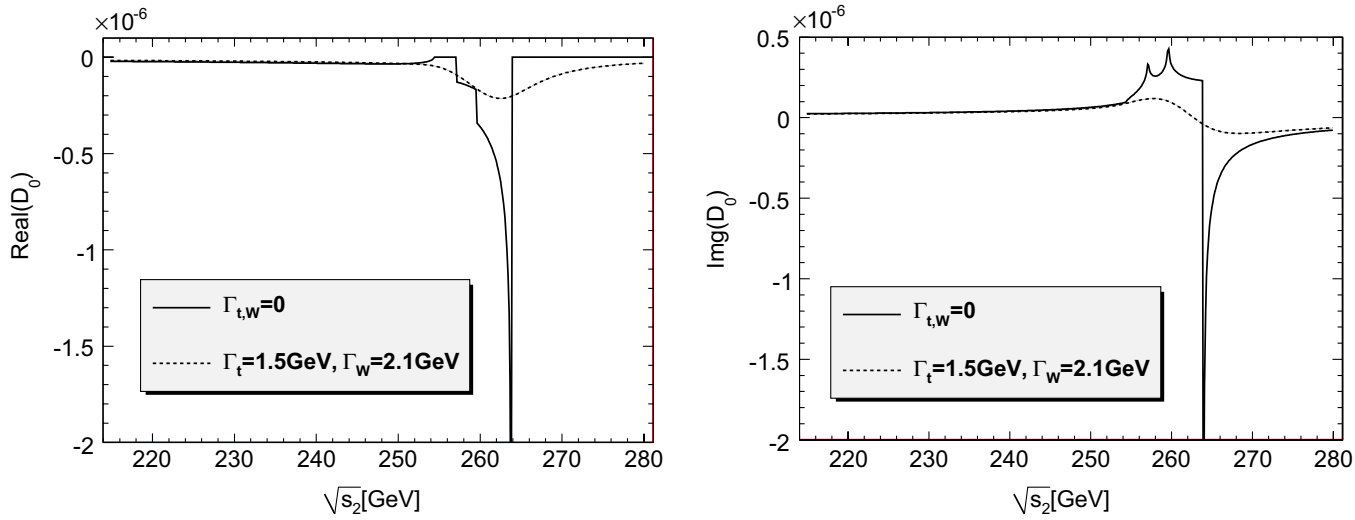

FIG. 10 (color online). Effect of the width of the W, Γ_W and of the top, Γ_t, on the real and imaginary part of the four-point scalar function.

would not only induce a width for the top but also for the W. Therefore to be realistic one should include the widths of both the top quark Γ_t, as well as the width of the W, Γ_W.

We take the simple prescription of a fixed width and make the substitution

$$m_t^2 \to m_t^2 - im_t\Gamma_t, \qquad M_W^2 \to M_W^2 - iM_W\Gamma_W. \tag{37}$$

Applied to the case of our four-point function, one sees in Fig. 10 that indeed the width regulates the LLS and gives a smooth result that nicely interpolates with the result at zero width away from the singularity. The normal threshold and the three-point subleading singularity are also softened. The real part of the four-point function still shows a smooth valley at the location of the LLS after regularization. For the imaginary part we note that after introducing the width the LLS singularity is drastically reduced with a contribution of the order of the subleading singularity.

As we will explain in the next section and in more detail in Appendix B the introduction of the width in a four-point function requires careful extension of the usual four-point function libraries. In the case at hand, as will be shown, the four-point function with complex internal masses can be written in an analytical form, albeit with a larger number of Spence functions compared to the case of real masses.

In our calculation of Yukawa corrections where all the relevant couplings depend only on the top-quark mass, the Higgs mass and the vacuum expectation value v, we will keep m_t, M_H, and v real while applying rules (37) to all the loop integrals.

One might ask whether the same prescription as in Eq. (37) for the Higgs mass can be of any relevance. A justification for this will require to consider the corresponding process including the Higgs decays with among other contributions, ''resonant contributions'' with an integration over the propagator of the Higgs. At least on a diagram by diagram basis this will not solve the problem since, for example, one still has to deal with the same four-point function but with M_H^2 replaced by a certain p_H^2, taking into account the fact the leading Landau singularity occurs for a wide range of Higgs masses and values of the invariant p_H^2. On the practical side, recall that compared to the top and W width of about 2 GeV, for Higgs masses of about $2M_W$ the width of the Higgs is 0.1 GeV, more than an order of magnitude smaller.[4]

V. IMPLEMENTATION OF COMPLEX MASSES IN THE LOOP INTEGRALS

We have implemented complex masses in all the loop integrals we encounter in calculating the cross section in the limit $\lambda_{bbH} = 0$ where the tree-level prediction vanishes. In this limit, we can also set the mass of the bottom quark to zero. In the $SU(3)$-gauge invariant classification of Fig. 2, class (a) vanishes in this approximation. In fact, we had shown [4] that even with $m_b = 4.62$ GeV class (a) is totally negligible. Although it is only class (c) that shows severe numerical instabilities due to the presence of a leading Landau singularity in the four-point box function and nonleading singularity in the five-point function we introduce the width in all diagrams of both classes (b) and (c).

[4]Our calculation of the leading Yukawa effects involves the charged Goldstone boson in the Feynman gauge through which the W mass enters. One may question whether it is appropriate to introduce a width here for a Goldstone boson considering that a Goldstone is defined as a massless state. Independently of the width one should first question why the Goldstone has a mass here. The point is in any other gauge than the Feynman gauge we would have had to consider the effect of the Goldstone and W exchange to derive the leading Yukawa effects. The physical thresholds are therefore captured in the Feynman gauge.

For the tensorial and scalar loop integrals with up to three legs we rely on LOOPTOOLS [13] which handles complex masses in up to three-point functions. The five-point functions are reduced to four-point functions according to [25,26]. The tensorial four-point functions are reduced to the scalar four-point function and three-point functions. We therefore have to calculate only the scalar four-point function with complex masses. The analytical calculation of the four-point function with complex masses in the most general case is practically intractable. If one of the external particles is lightlike, the standard technique of 't Hooft and Veltman [27] brings some light although the result writes in terms of 72 Spence functions. In our example, $gg \to b\bar{b}H$ with massless bottom quarks, there are at least 2 lightlike external momenta in all boxes, including the ones derived from the pentagon diagrams. If the positions, in the box, of two lightlike momenta are opposite then we can write the result in terms of 32 Spence functions. If the two lightlike momenta are adjacent, the result contains 60 Spence functions. The detailed derivation and results are given in Appendix B. We have implemented those analytical formulae for the case of two massless external momenta into a code and added this into LOOPTOOLS.[5]

We have performed a variety of checks on the new loop integrals with complex internal masses. First of all, for *all* the tensorial and scalar loop integrals (four- and five-point functions), we have performed a trivial numerical consistency check making sure that as the numerical value of the widths is negligibly small, widths $\to 0^+$, one recovers the well-tested result with real internal masses. For the scalar loop integrals, the results are compared to the ones calculated numerically in the limit of large widths, e.g. $\Gamma_{t,W} = 100$ GeV, and we find an excellent agreement. Furthermore, for the scalar box integrals the results can be checked by using the segmentation technique described in [28]. The idea is the following. At the boundary of phase space where the Gram determinant vanishes, the four-point function can be written as a sum of 4 three-point functions. The three-point functions with complex masses can be calculated by usingLOOPTOOLS . In this way, we have verified with excellent precision that the results of the scalar four-point functions are correct at the boundary of phase space. We have also carried out a comparison with a dedicated purely numerical approach based on an extension of the extrapolation technique [29]. We have found perfect agreement.[6]

In a second stage, we have performed checks at the amplitude level. A very trivial one was to check that the results with the new loop library exactly match the ones with the standard loop library with real masses in the limit widths $\to 0^+$. Another important check was to verify that the results calculated with complex internal masses are QCD gauge invariant; see [4] for this check.

Since the leading Landau singularity is integrable at interference level, the NLO calculation with $\lambda_{bbH} \neq 0$ performed in [4] can be trivially extended to the region of $M_H \geq 2M_W$ by using the same method without introducing widths for unstable internal particles. However, there is a small problem related to the universal correction $(\delta Z_H^{1/2} - \delta v)$ where the wave function renormalization of the Higgs $\delta Z_H^{1/2}$ related to the derivative of the Higgs two-point function becomes singular when M_H equal to $2M_W$ or $2M_Z$ [30]. We regularize this singularity by separately introducing the widths of the W and the Z. This singularity, contrary to the leading Landau singularity, is due to the Higgs being an external one-shell particle. Other ways for dealing with this problem have been discussed [31].

VI. INPUT PARAMETERS AND KINEMATICAL CUTS

The input parameters are the same as given in [4]. We rewrite them here together with new inputs which are the widths of the unstable particles appearing in the calculation.

$$\begin{aligned} &\alpha(0) = 1/137.03599911, \qquad \alpha_s(M_Z) = 0.118, \\ &M_W = 80.3766 \text{ GeV} (G_\mu = 1.16639 \times 10^{-5} \text{ GeV}^{-2}), \\ &M_Z = 91.1876 \text{ GeV}, \qquad m_t = 174.0 \text{ GeV}, \\ &\Gamma_W = 2.1 \text{ GeV}, \qquad \Gamma_Z = 2.4952 \text{ GeV}. \end{aligned} \tag{38}$$

The top-quark width is calculated at the tree level in the standard model as

$$\Gamma_t = \frac{G_\mu (m_t^2 - M_W^2)^2 (m_t^2 + 2M_W^2)}{8\pi\sqrt{2} m_t^3} \approx 1.5 \text{ GeV}, \tag{39}$$

where the bottom-quark mass has been neglected. The Cabibbo-Kobayashi-Maskawa parameter V_{tb} is set to be 1. Most of our discussion concerns the most interesting case of the limit $\lambda_{bbH} \to 0$, where as we have discussed at length (see also [4]), the effect of the b-quark mass other than in the Higgs coupling is totally negligible. Therefore we set this mass to zero when discussing this limit in Sec. VII. For completeness we will also give results for the NLO corrections in Sec. VIII which require $\lambda_{bbH} \neq 0$. There we will set $m_b = 4.62$ GeV. When we refer to the leading order contribution we will have in mind the cross section at the Born level calculated with $m_b = 4.62$ GeV. The cross section from the one-loop amplitude squared with $\lambda_{bbH} \to 0$ will, in a few instances, be normalized to this Born cross section to give a measure of the new electroweak effect and so as to allow comparison with the NLO corrections.

[5]The implementation for the case of one massless external momentum is straightforward. However, we have not done this yet since it is not necessary for our present calculation.

[6]We thank F. Yuasa for sending us the results of the extrapolation technique.

We consider the case at the LHC where the pp center of mass energy is $\sqrt{s} = 14$ TeV. Neglecting the small light quark initiated contribution (see [4]), we use CTEQ6L [32–35] for the gluon density function in the proton. The factorization scale for this density and the energy scale for the strong coupling constant are both chosen to be $Q = M_Z$ for simplicity.

As has been done in previous analyses [4,14,15], for the exclusive $b\bar{b}H$ final state, we require the outgoing b and $\bar{b}$ to have high transverse momenta $|\mathbf{p}_T^{b,\bar{b}}| \geq 20$ GeV and pseudorapidity $|\eta^{b,\bar{b}}| < 2.5$. These kinematical cuts reduce the total rate of the signal but also greatly reduce the QCD background. As pointed in [16] these cuts also stabilize the scale dependence of the QCD NLO corrections compared to the case where no cut is applied. In the following, these kinematical cuts are always applied.

VII. RESULTS IN THE LIMIT OF VANISHING λ_{bbH}

A. Total cross section

We start with the cross section in the case where $\lambda_{bbH} = 0$. In [4], we reported on results up to $M_H = 150$ GeV that showed that this cross section was rising fast as one approached the threshold $M_H = 2M_W$. Beyond this threshold our integrated cross sections showed large instabilities. As we discussed in Sec. III this is due to the appearance of a leading singularity which as we have advocated can be cured by the introduction of a width for the unstable top quark and W gauge boson. We also showed in Sec. III that the region of Landau singularity spans the region $2M_W \leq M_H \leq 211$ GeV with $2m_t < \sqrt{s_{gg}} = \sqrt{s} \leq 457$ GeV; see Fig. 8. Before convoluting with the gluon distribution let us briefly look at the behavior of the partonic cross section $gg \rightarrow b\bar{b}H$, paying a particular attention to this leading Landau singularity region.

Figures 11 show that indeed the widths do regulate the cross section. Moreover it is within this range that the cross section is largest even after being regulated. The (highest) peak of the cross section occurs for a Higgs mass of 163 GeV about Γ_W above the $M_H = 2M_W$ threshold, and for $\sqrt{s} = 351$ GeV about $2\Gamma_t$ above the $\sqrt{s} = 2m_t$ threshold. Figures 11 show that the cross section exhibits a peak structure close to the onset of the normal thresholds in M_H, $\sqrt{s}$ even when one is slightly outside the leading Landau singularity region of the four-point function. In fact, this enhancement at the normal threshold is far from being totally due the four-point LLS especially after the latter has been regularized by the introduction of the width. At the normal threshold there is an enhancement from the accumulation of all the two-point, three-point, and, of course, the four-point function. Moreover as we noted in Sec. IV (see Fig. 10), the introduction of the widths brings the contribution of the LLS to the level of a subleading singularity.

The cross section at the pp level for the 14 TeV center of mass energy at the LHC as a function of the Higgs mass is shown in Fig. 12, taking into account the width of the top quark and the W gauge boson. For comparison we also show the cross section without the width effect outside the leading Landau singularity range of M_H. The sharp rise above $M_H > 150$ GeV is nicely tamed. On the other hand, note that on leaving the leading Landau singularity region around $M_H = 211$ GeV, the width effect is much smaller and the figures suggest that one could have ''entered this region from the right'' without having recourse to introducing a width. Indeed our numerical integration routine over phase space with the default LOOPTOOLS library does not show as bad behavior until we venture around values of $2M_W \leq M_H < 200$ GeV. The reason for this can be understood by taking a glance at Fig. 8. For 200 GeV $< M_H <$ 211 GeV the singularity region is considerably shrunk to a

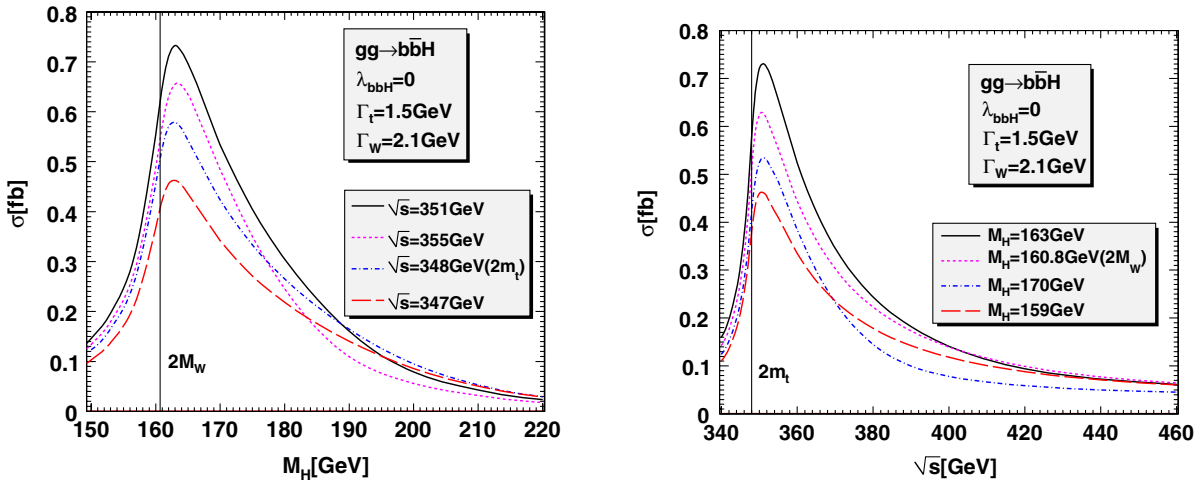

FIG. 11 (color online). Left panel: the cross section for the subprocess $gg \rightarrow b\bar{b}H$ as functions of M_H for various values of $\sqrt{s}$ including the case $\sqrt{s} = 2m_t = 348$ GeV. Right panel: the cross section for the subprocess $gg \rightarrow b\bar{b}H$ as functions of $\sqrt{s}$ for various values of M_H including the case $M_H = 2M_W = 160.7532$ GeV.

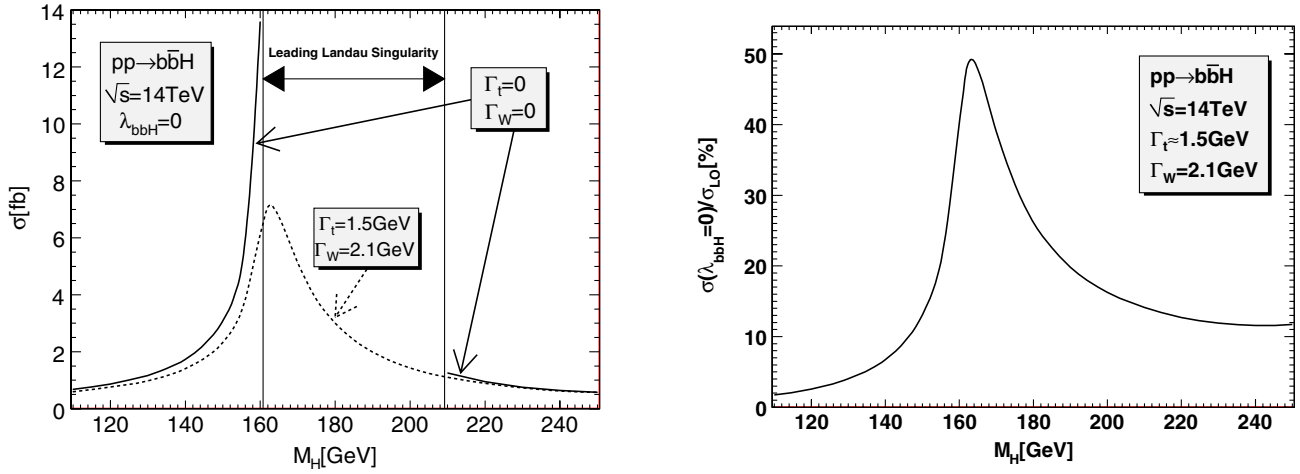

FIG. 12 (color online). Left panel: the one-loop induced cross section as a function of M_H in the limit of vanishing bottom-Higgs Yukawa coupling for two cases: with and without widths. Right panel: the percentage correction of the contribution with widths relative to the tree-level cross section calculated with $\lambda_{bbH} \neq 0$.

line so that one is integrating over an almost zero measure. The effect of the widths outside the singularity region is to reduce the cross section for $M_H = 120$ GeV, 140 GeV, and 150 GeV by, respectively, 15%, 24%, and 33% while for $M_H = 210$ GeV, 230 GeV, and 250 GeV the reduction is comparatively more modest with, respectively, 15%, 5%, and 2%.

Normalized to the Born cross section the new contribution represents a mere 2.6% for $M_H = 120$ GeV. It increases, however, to as much as 49% for $M_H = 163$ GeV before stabilizing to about 10% for larger Higgs masses.

B. Distributions

Since the effect of the new purely one-loop contribution is as large as ~50% (compared to the Born cross section even after being regulated through the introduction of the widths), it is essential that one looks at different distributions to see if this new effect can be described as a simple K factor. The two examples we show for $M_H = 150$ GeV (before the onset of the leading Landau singularity) and for $M_H = 163$ GeV, where the effect on the total cross section are largest, show that the corrections are not uniformly distributed for all distributions. Figures 13 and 14 for $M_H = 150$ GeV show the effect of the width. While the relative difference is rather uniform, about 33%, on the Higgs pseudorapidity η_H distribution, the transverse momentum distributions of the Higgs p_T^H, and the bottom p_T^b are strongly affected, in particular, for values which in the absence of the width showed a peak structure. There is still some peak structure in the p_T distributions but the width effect reduces this by as much as 50%, while in the tails it is about 10%.

Let us now turn to $M_H = 163$ GeV. The correction, normalized to the Born cross section, for the Higgs pseudorapidity distribution is about 60% around the center region. The corrections to the p_T distributions can be enormous in some regions of phase space, up to 200% for the Higgs and about 170% for the bottom-quark case. These huge corrections to the distributions in some region of phase space are again due to the effect of Landau singularities.

One may question whether these large corrections signal the breakdown of perturbation theory and whether one expects (even) higher order effects to be large. We do not think so. First of all, the relative large corrections have to do with the fact that for vanishing λ_{bbH} the tree-level cross section vanishes. Second, higher order effects have been captured in the introduction of the width and there is no reason to suspect that the leading Landau singularity we have encountered is affected by higher order effects.

VIII. RESULTS AT NLO WITH $\lambda_{bbH} \neq 0$

The results of the electroweak corrections at NLO which represent the interference contribution between the Born and the one-loop amplitude are much less interesting and numerically quite small, a trend that we had found already when studying at some length the electroweak NLO for $M_H < 150$ GeV [4]. Moreover, although some one-loop diagrams contain a leading Landau singularity at the interference level this singularity as we have shown in Sec. III is integrable; see Eq. (11). The NLO contribution, apart from the Higgs wave function renormalization effect, is numerically stable even if one does not implement widths of the internal particles. The purpose of this section is to briefly present the results for the NLO. We first show that the effect of introducing the width is very small then show the NLO result without the internal widths being implemented hence these results are genuinely NLO results. These results thus complement the study we made for $M_H <$ 150 GeV [4].

As discussed in Sec. II, the NLO Yukawa corrections consist of 3 QCD gauge invariant classes; see Fig. 2. Class

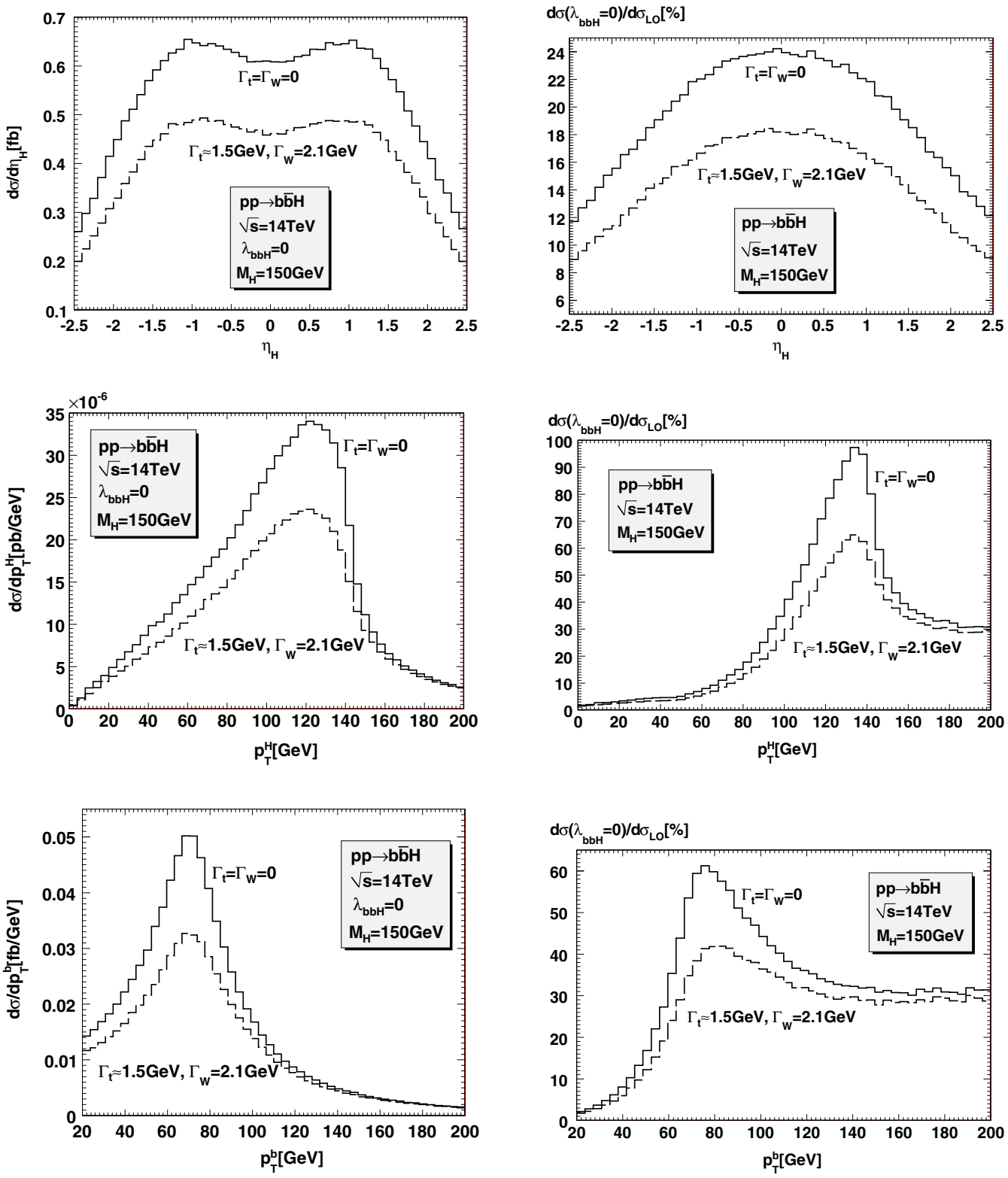

FIG. 13 (color online). The pseudorapidity of the Higgs and transverse momentum distributions of the Higgs and the bottom for $M_H = 150$ GeV arising from the purely one-loop contribution in the limit of vanishing LO ($\lambda_{bbH} = 0$) for two cases: with and without widths. The relative percentage contribution $d\sigma(\lambda_{bbH} = 0)/d\sigma_{\mathrm{LO}}$ is also shown.

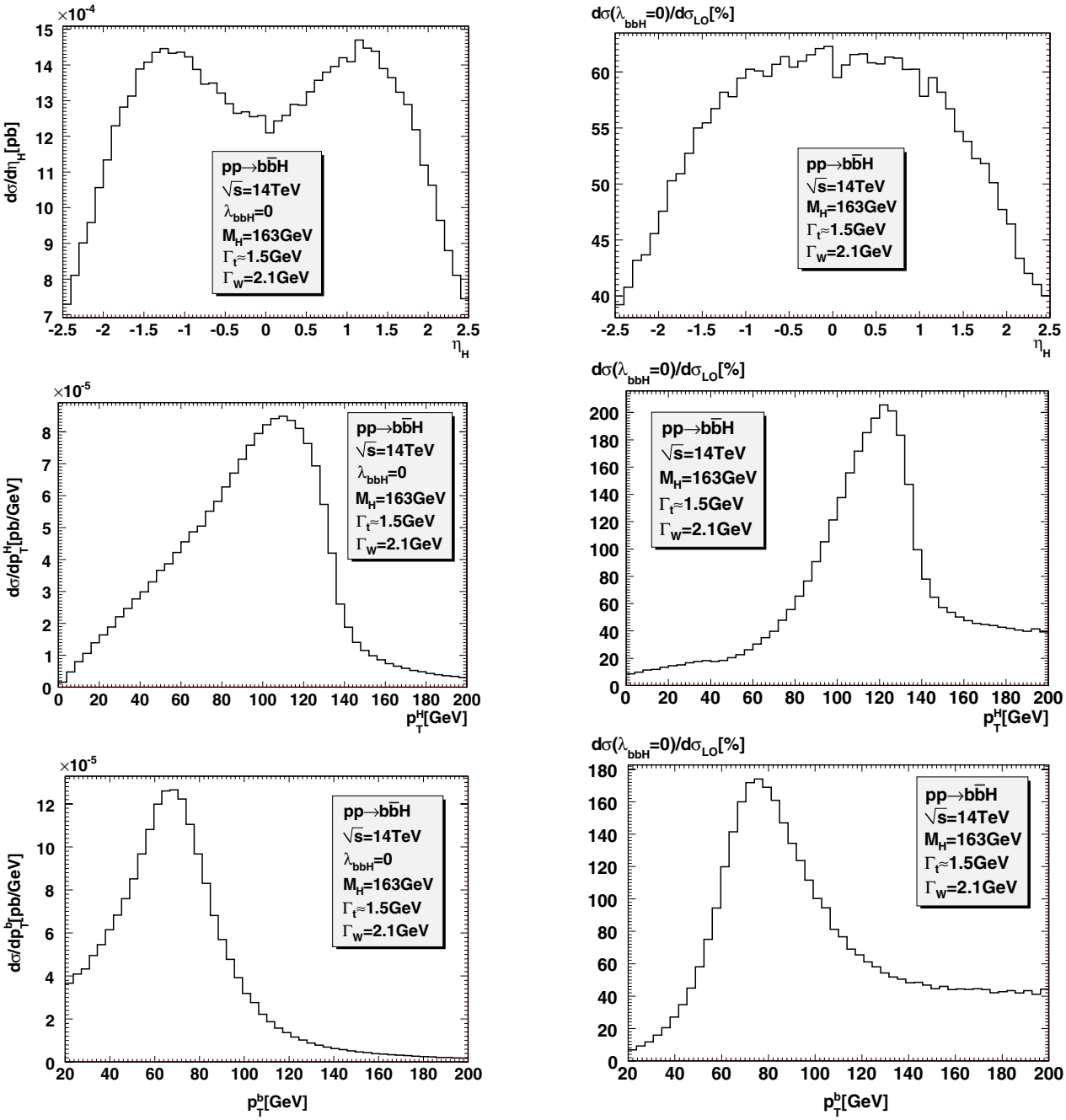

FIG. 14 (color online). The pseudorapidity of the Higgs and transverse momentum distributions of the Higgs and the bottom for $M_H = 163$ GeV arising from the purely one-loop contribution in the limit of vanishing LO ($\lambda_{bbH} = 0$). Its relative percentage contribution $d\sigma(\lambda_{bbH} = 0)/d\sigma_{\rm LO}$ is also shown.

(a) gives a totally negligible correction below 0.1%. We will not discuss this contribution any further here. Moreover, the leading Landau singularity we have discussed only shows up in class (c). As a first step we therefore study the NLO correction due to class (c) and weigh the effect of implementing the width of the internal particles. Class (b) does not develop a leading Landau singularity and therefore the width effects will be marginal. Another correction with enhanced Yukawa coupling is the universal correction, $(\delta Z_H^{1/2} - \delta v)$ where $\delta Z_H^{1/2}$, the Higgs wave function renormalization constant involving the derivative of the two-point function Higgs self-energy. The latter is ill defined when M_H is equal to $2M_W$ or $2M_Z$. Here the width of all unstable particles, W, Z, t, will be kept.[7]

[7]Note that $\delta Z_H^{1/2}$ does not diverge when $M_H = 2m_t$ and the top-quark width thus has a marginal effect on $\delta Z_H^{1/2}$.

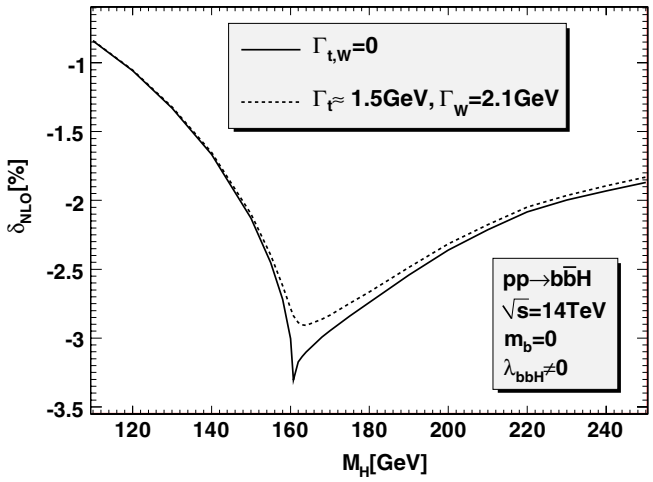

FIG. 15 (color online). Contribution of class (c) at NLO. The one-loop amplitude is calculated by keeping m_b only in the λ_{bbH} coupling.

A. Width effect at NLO

Our implementation of the width in the four-point function has been done in the limit of massless external quarks. To be fully consistent in the calculation of the one-loop amplitude with widths using the modified four-point function we switch off the bottom mass in the spinors and propagators but keep $\lambda_{bbH} \neq 0$ as an independent parameter. Our result for the NLO contribution of class (c) is shown in Fig. 15. First of all, as we can see the overall correction is quite small, even at the onset of the (integrable) leading Landau singularity, the correction to the Born term is below 3.5%. The existence of a dip at the expected location is noticeable. Width effect softens the dip behavior somehow but the effect is not as dramatic as what we have seen in the previous section for the loop squared results. We find that if $M_H < 158$ GeV or $M_H > 165$ GeV then the width effects change the NLO result but not more than 5%, and are therefore totally negligible especially if one takes into account the smallness of the NLO result itself. Therefore the full NLO results can be studied by safely neglecting the width effect in classes (b) and (c).

B. NLO corrections with $m_b \neq 0$

The results for the NLO corrections are shown in Fig. 16 as a function of the Higgs mass. We implement widths only in the two-point function wave function renormalization of the Higgs. The latter contributes an almost constant -1% correction apart from oscillations in the range $2M_W$ to $2M_Z$ due to the dips at $2M_W$ and $2M_Z$ where the Higgs wave function is not analytic at those values. The effect of the widths of the W and Z smooths the behavior and the correction is never larger than 3.5% in this range of Higgs masses. The contribution from class (b) where the Higgs couples to the internal top decreases very slowly as the Higgs mass increases from 110 to 250 GeV; as expected, there is no structure as would be the case if this contribution were sensitive to any threshold or singularity. Class (c) on the other hand does, as expected, reveal some structure around $M_H = 2M_W$ where we see a fall in the relative correction. The correction is however, despite this fall, quite modest ranging from $\sim -1\%$ for $M_H = 160$ GeV to -4% for $M_H = 210$ GeV. When we studied the effect of the width of the internal particles on class (c) at NLO, we did so in the massless quark limit. In that limit, the outgoing quarks have opposite helicity so that only the $\delta_{\lambda_3,-\lambda_4}$ helicity amplitude survives; $\lambda_{3,4}$ are the quark helicities. In our case here when the quark mass is reinstated, the $\delta_{\lambda_3,\lambda_4}$ helicity amplitude switches on. Figure 16

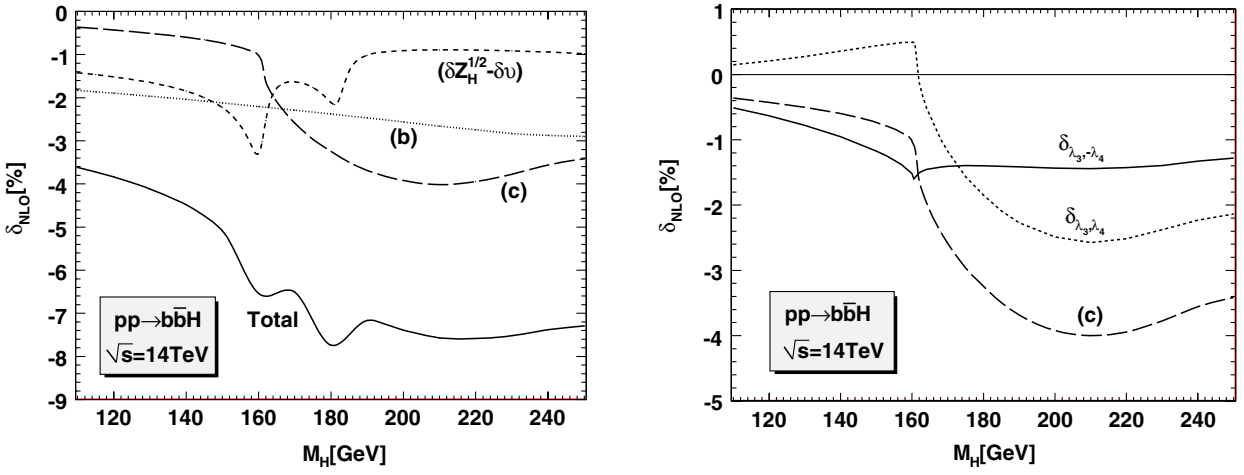

FIG. 16 (color online). Left panel: The relative NLO electroweak corrections normalized to the tree-level cross section. (b) and (c) correspond to the two classes of diagrams displayed in Fig. 2. $(\delta Z_H^{1/2} - \delta v)$ is the universal correction contained in the renormalization of the $b\bar{b}H$ vertex. "Total" refers to the sum of those 3 corrections. $\delta Z_H^{1/2}$ is calculated by taking into account the widths of W, Z, and the top quark. Right panel: the structure of (c)-correction which is a sum of two independent helicity configurations.

(right) shows that these two helicity amplitudes behave differently as a function of the Higgs mass. The effect of the b-quark mass makes the dip in the $\delta_{\lambda_3,-\lambda_4}$ much softer that in the massless case displayed in Fig. 15. In the $\delta_{\lambda_3,\lambda_4}$, the fall of the correction around $M_H = 2M_W$ is more apparent. This is another manifestation of how the dynamics can affect the structure of a singularity.

Adding the effect of all the contributions at NLO the total correction changes from -4% for $M_H = 110$ GeV to -8% at $M_H \sim 2M_Z$ stabilizing to around -7% past this value up to $M_H = 250$ GeV.

IX. CONCLUSIONS

At tree-level, Higgs production in association with a b-quark pair at the LHC is dominated by $gg \to b\bar{b}H$, where the Higgs is radiated from the b quark with a strength proportional to the bottom-Higgs Yukawa coupling. Unfortunately in the standard model this coupling is extremely small and therefore this mechanism is not a Higgs discovery channel, although once the Higgs has been found the study of the Higgs coupling to the b quark through this reaction could probe interesting phenomena having to do with the mechanism of symmetry breaking and the role played by the third generation fermions. Electroweak one-loop effects are usually small compared to the QCD corrections, however processes involving the bottom quark, electroweak one-loop corrections involve the top quark whose Yukawa coupling is of the order the QCD strength. More interesting for $b\bar{b}H$ production is that even in the limit where the bottom-Higgs Yukawa coupling vanishes and therefore the Born tree-level cross section vanishes, electroweak one-loop effects, through the top-Higgs Yukawa coupling, in particular, can still trigger this reaction. We studied these effects in some detail in a previous publication [4] but presented results for Higgs masses below $2M_W$. We remarked that for the one-loop contribution in the limit of vanishing bottom-Higgs Yukawa coupling, the cross section was growing as the Higgs mass increased and that numerical results started showing instabilities past $M_H \geq 2M_W$. The aim of this paper was to extend the study performed in [4] to the mass range where numerical instabilities occurred. The origin of the numerical instabilities is due to the fact that some one-loop contributions, contained in some box diagrams, develop a leading Landau singularity. We have here reviewed in some detail the problem of the occurrence of the leading Landau singularity and investigated in more details the conditions and dynamics as concerns $b\bar{b}H$ production. Since this singularity is not integrable when the one-loop amplitude is squared, we regulate the cross section by taking into account the width of the internal top and W particles. This requires that we extend the usual box one-loop function to the case of complex masses. We show how this can be implemented analytically in our case. We study in some detail the cross section at the LHC as a function of the Higgs mass and show how some distributions can be drastically affected compared to the tree-level result. For completeness we have also extended our study of the NLO Yukawa electroweak corrections which represent the interference between the one-loop amplitude and the tree-level amplitude. At this level the Landau singularity is integrable and therefore does not require that one endows the internal particle with a width. The NLO correction is found to be small.

ACKNOWLEDGMENTS

L. D. N. expresses his gratitude and thanks to P. Aurenche for his support, most helpful discussions and comments. We benefited a lot from discussions with G. Altarelli, C. Bernicot, DO Hoang Son, J. Fujimoto, J. P. Guillet, K. Kato, Y. Kurihara, E. Pilon and F. Yuasa. Special thanks go to F. Yuasa for comparisons between her numerical code and our code for the four-point function with complex masses. We thank A. Denner for his many useful comments related to the manuscript. L. D. N. acknowledges the financial support of *Rencontres du Vietnam*.

APPENDIX A: NATURE OF THE LEADING LANDAU SINGULARITY

We give in this section more detail about our derivation of Eq. (10). One can rewrite Eq. (2) in the form

$$T_0^N = \Gamma(N) \int_0^\infty dx_1 \cdots dx_N \delta\Big(\sum_{i=1}^N x_i - 1\Big) \times \int \frac{d^D q}{(2\pi)^D i} \frac{1}{(q^2 - \Delta)^N}, \tag{A1}$$

where

$$\Delta = \frac{1}{2} \sum_{i,j=1}^N x_i x_j Q_{ij} - i\varepsilon \tag{A2}$$

with Q_{ij} given in Eq. (6). Integrating over q gives

$$T_0^N = \frac{(-1)^N \Gamma(N - D/2)}{(4\pi)^{D/2}} \int_0^1 dx_1 \cdots dx_N \frac{\delta(\sum_{i=1}^N x_i - 1)}{\Delta^{N-D/2}}. \tag{A3}$$

The Landau equations for the representation (A3) are [6]

$$\begin{cases} \Delta = 0, \\ \frac{\partial \Delta}{\partial x_i} = 0. \end{cases} \tag{A4}$$

Since Δ is a homogeneous function of x_i, the first equation in (A4) is automatically satisfied when the second is. Equation (A4) is equivalent to Eq. (5), which means that the solution of Eq. (A4) is an eigenvector of Q with zero eigenvalue. In general, Q has N real eigenvalues $\lambda_1, \ldots, \lambda_N$. The characteristic equation of Q is given by

$$f(\lambda) = \lambda^N + (-1)a_{N-1}\lambda^{N-1} + (-1)^2 a_{N-2}\lambda^{N-2} - \ldots (-1)^{N-1} a_1 \lambda + (-1)^N a_0 = (\lambda - \lambda_1)(\lambda - \lambda_2)\ldots(\lambda - \lambda_n) = 0. \quad \text{(A5)}$$

For the case $N = 4$ we have

$$a_0 = \lambda_1\lambda_2\lambda_3\lambda_4 = \det(Q_4),$$
$$a_1 = \lambda_1\lambda_2\lambda_3 + \lambda_1\lambda_2\lambda_4 + \lambda_1\lambda_3\lambda_4 + \lambda_2\lambda_3\lambda_4,$$
$$a_2 = \lambda_1\lambda_2 + \lambda_1\lambda_3 + \lambda_1\lambda_4 + \lambda_2\lambda_3 + \lambda_2\lambda_4 + \lambda_3\lambda_4,$$
$$a_3 = \lambda_1 + \lambda_2 + \lambda_3 + \lambda_4 = \mathrm{Tr}(Q_4). \quad \text{(A6)}$$

Consider the case where Q has only one very small eigenvalue $\lambda_N \ll 1$, then to a very good approximation

$$\lambda_N \simeq \frac{a_0}{a_1}, \qquad a_1 = \lambda_1\lambda_2\ldots\lambda_{N-1} \neq 0. \quad \text{(A7)}$$

Let $V = \{x_1^0, x_2^0, \ldots, x_N^0\}$ be the eigenvector corresponding to the eigenvalue λ_N. V is normalized to

$$\sum_{i=1}^{N} x_i^0 = 1. \quad \text{(A8)}$$

For latter use, we define

$$v^2 = V.V. \quad \text{(A9)}$$

The expansion of Δ around V reads

$$\Delta = \frac{1}{2}\sum_{i,j=1}^{N} Q_{ij} y_i y_j + \lambda_N \sum_{i=1}^{N} x_i^0 y_i + \frac{1}{2}\lambda_N v^2 - i\varepsilon, \quad \text{(A10)}$$

where $y_i = x_i - x_i^0$. In order to find the leading singularity, it will be sufficient to neglect the linear term in the right-hand side. The Q matrix can be diagonalized by rotating the y vector

$$y_i = \sum_{j=1}^{N} A_{ij} z_j, \quad \text{(A11)}$$

where A is an orthogonal matrix whose columns are the normalized eigenvectors of Q. Thus we have

$$\det(A) = 1, \qquad \sum_{j=1}^{N} A_{Nj} = \frac{\sum_{i=1}^{N} x_i^0}{\sqrt{V.V}} = \frac{1}{v},$$
$$\Delta = \frac{1}{2}\sum_{i=1}^{N-1} \lambda_i z_i^2 + \frac{1}{2}\lambda_N v^2 - i\varepsilon. \quad \text{(A12)}$$

Note that the term $\lambda_N z_N^2$ in the right-hand side has been neglected as this term would give a contribution of the order $\mathcal{O}(\lambda_N^2)$ to the final result. Equation (A3) can now be rewritten in the form

$$T_0^N = \frac{(-1)^N \Gamma(N - D/2)}{\pi^{D/2} 2^{3D/2-N}} \int_{-\infty}^{+\infty} dz_1 \cdots dz_N \times \frac{\delta(\sum_{i,j=1}^{N} A_{ij} z_j)}{(\sum_{i=1}^{N-1} \lambda_i z_i^2 + \lambda_N v^2 - i\varepsilon)^{N-D/2}}. \quad \text{(A13)}$$

Although the original integration contour is some segment around the singular point $z_i = 0$ with $i = 1, \ldots, N$, the singular part will not be changed if we extend the integration contour to infinity, provided the power $(N - D/2)$ of the denominator in Eq. (A13) is sufficiently large. Integrating over z_N gives

$$T_0^N = \frac{(-1)^N \Gamma(N - D/2) v}{\pi^{D/2} 2^{3D/2-N}} \int_{-\infty}^{+\infty} dz_1 \cdots dz_{N-1} \times \frac{1}{(\sum_{i=1}^{N-1} \lambda_i z_i^2 + \lambda_N v^2 - i\varepsilon)^{N-D/2}}, \quad \text{(A14)}$$

where the factor v comes from the δ function. Assuming that $\lambda_i > 0$ for $i = 1, \ldots, K$ and $\lambda_j < 0$ for $j = K + 1, \ldots, N - 1$ with $0 \leq K \leq N - 1$, we change the integration variables as follows:

$$\begin{cases} t_i = \sqrt{\lambda_i} z_i & \text{for } i = 1, \ldots K, \\ t_j = \sqrt{-\lambda_j} z_j & \text{for } j = K + 1, \ldots N - 1. \end{cases} \quad \text{(A15)}$$

This makes sure that all t_i are real. We get

$$T_0^N = \frac{(-1)^N \Gamma(N - D/2) v}{\pi^{D/2} 2^{3D/2-N} \sqrt{(-1)^{N-K-1} a_1}} \times \int_{-\infty}^{+\infty} dt_1 \cdots dt_K \times \int_{-\infty}^{+\infty} dt_{K+1} \cdots dt_{N-1} \frac{1}{(-\sum_{i=K+1}^{N-1} t_i^2 + b^2)^{N-D/2}}, \quad \text{(A16)}$$

where

$$b^2 = \sum_{i=1}^{K} t_i^2 + \lambda_N v^2 - i\varepsilon, \qquad \mathrm{Re}(b^2) > 0. \quad \text{(A17)}$$

Changing to spherical coordinates and using the following formulae for the volume

$$\int_{-\infty}^{+\infty} dt_1 \cdots dt_K = \int_0^{\infty} r^{K-1} dr d\Omega_{K-1}, \qquad \int d\Omega_{K-1} = \frac{2\pi^{K/2}}{\Gamma(K/2)}, \quad \text{(A18)}$$

we arrive at

$$T_0^N = \frac{(-1)^N \Gamma(N - D/2) v}{\pi^{D/2} 2^{3D/2-N} \sqrt{(-1)^{N-K-1} a_1}} \frac{2\pi^{(N-K-1)/2}}{\Gamma((N - K - 1)/2)} \times \int_{-\infty}^{+\infty} dt_1 \cdots dt_K \int_0^{\infty} dr \frac{r^{N-K-2}}{(b^2 - r^2)^{N-D/2}}. \quad \text{(A19)}$$

Note that $(b^2 - r^2)^{N-D/2} = e^{-i\pi(N-D/2)}(r^2 - b^2)^{N-D/2}$ due to the fact that $\varepsilon > 0$. Using

$$\int_0^{\infty} ds \frac{s^{\alpha-1}}{(z + s)^{\beta}} = z^{(\alpha-\beta)} \frac{\Gamma(\beta - \alpha)\Gamma(\alpha)}{\Gamma(\beta)}, \quad \text{(A20)}$$

gives

$$T_0^N = \frac{(-1)^N e^{i\pi(N-K-1)/2} v}{\pi^{D/2} 2^{3D/2-N} \sqrt{(-1)^{N-K-1} a_1}} \pi^{(N-K-1)/2} \times \Gamma((N - D + K + 1)/2) \times \int_{-\infty}^{+\infty} dt_1 \cdots dt_K \times \frac{1}{(\sum_{i=1}^{K} t_i^2 + \lambda_N v^2 - i\varepsilon)^{(N-D+K+1)/2}}. \quad \text{(A21)}$$

Repeat the above steps to write

$$T_0^N = \frac{(-1)^N e^{i\pi(N-K-1)/2}\upsilon}{2^{3D/2-N}\sqrt{(-1)^{N-K-1}a_1}} \times \frac{\pi^{(N-D-1)/2}\Gamma((N-D+1)/2)}{(\lambda_N \upsilon^2 - i\varepsilon)^{(N-D+1)/2}}. \quad \text{(A22)}$$

This result was derived with the condition

$$a_1 \neq 0 \quad \text{and} \quad N - D + 1 > 0. \quad \text{(A23)}$$

However it can be trivially analytically continued if we work in $D = 4 - 2\epsilon$ so that it applies to $N \leq 3$ in $D = 4$ by taking the limit $\epsilon \to 0$. Alternatively, with $D = 4$ and $N = 3$ the scalar function

$$T_0^3 = \frac{-\upsilon}{8\pi^2}\int dz_1 dz_2 \frac{1}{(\lambda_1 z_1^2 + \lambda_2 z_2^2 + \lambda_3 \upsilon^2 - i\varepsilon)}. \quad \text{(A24)}$$

One first needs to dispose of the ultraviolet divergent. To that effect we differentiate the above equation with respect to $\eta = \lambda_3 \upsilon^2$ with the result

$$\frac{dT_0^3}{d\eta} = \frac{\upsilon}{8\pi^2}\int_{-\infty}^{\infty} dz_1 dz_2 \frac{1}{(\lambda_1 z_1^2 + \lambda_2 z_2^2 + \eta - i\varepsilon)^2} = \frac{e^{i\pi(2-K)/2}\upsilon}{8\pi\sqrt{(-1)^{2-K}\lambda_1\lambda_2}} \frac{1}{\eta - i\varepsilon}. \quad \text{(A25)}$$

Integrating back (with respect to η) we get

$$T_0^3 = \frac{e^{i\pi(2-K)/2}\upsilon}{8\pi\sqrt{(-1)^{2-K}\lambda_1\lambda_2}} \ln(\lambda_3 \upsilon^2 - i\varepsilon) + C, \quad \text{(A26)}$$

where C is a constant independent of η. This result coincides with Eq. (12).

APPENDIX B: SCALAR BOX INTEGRALS WITH COMPLEX MASSES

The derivation of the analytical expression of the scalar one-loop function for the box ($N = 4$) with complex internal masses in the most general case with no restriction on the external invariants is not tractable. However, if at least one of the invariant masses of the external legs is lightlike one can derive an analytical formula in closed form starting from the standard approach of 't Hooft and Veltman [27] (see also [36]). For our application there are at least 2 lightlike external momenta in all boxes. We explain here our derivation based on the method given in [27] for this special case.

The scalar box integral is deduced from Eq. (A3) with x_4 integrated out with the result

$$D_0 \equiv (4\pi)^2 T_0^4 = \int_0^1 dx \int_0^x dy \int_0^y dz \frac{1}{(ax^2 + by^2 + gz^2 + cxy + hxz + jyz + dx + ey + kz + f)^2}, \quad \text{(B1)}$$

where we have changed the integration variables as $t = \sum_{i=1}^4 x_i$, $x = \sum_{i=1}^3 x_i$, $y = x_1 + x_2$, $z = x_1$; and

$$\begin{aligned} a &= \frac{1}{2}(Q_{33} + Q_{44} - 2Q_{34}) = p_3^2, \qquad b = \frac{1}{2}(Q_{22} + Q_{33} - 2Q_{23}) = p_2^2, \\ g &= \frac{1}{2}(Q_{11} + Q_{22} - 2Q_{12}) = p_1^2, \qquad c = Q_{23} + Q_{34} - Q_{33} - Q_{24} = 2p_2.p_3, \\ h &= Q_{13} + Q_{24} - Q_{14} - Q_{23} = 2p_1.p_3, \qquad j = Q_{12} + Q_{23} - Q_{22} - Q_{13} = 2p_1.p_2, \\ d &= Q_{34} - Q_{44} = m_3^2 - m_4^2 - p_3^2, \qquad e = Q_{24} - Q_{34} = m_2^2 - m_3^2 - p_2^2 - 2p_2.p_3, \\ k &= Q_{14} - Q_{24} = m_1^2 - m_2^2 + p_1^2 + 2p_1.p_4, \qquad f = \frac{Q_{44}}{2} - i\varepsilon = m_4^2 - i\varepsilon, \end{aligned} \quad \text{(B2)}$$

with Q_{ij} is defined in Eq. (6). Our application will be to complex masses, m_i^2, with $i = 1, 2, 3, 4$, d, e, k, f are therefore complex parameters while other parameters are real. The two lightlike external momenta can be either adjacent or opposite to each other. We consider in each of these two cases separately.

1. Integral with two opposite lightlike external momenta

For the box shown in Fig. 17 with $p_1^2 = p_3^2 = 0$ one gets $a = g = 0$ and writes

$$D_0^{(13)} = \int_0^1 dx \int_0^x dy \int_0^y dz \frac{1}{(by^2 + cxy + hxz + jyz + dx + ey + kz + f)^2}. \quad \text{(B3)}$$

Integrating over z to get

$$D_0^{(13)} = \int_0^1 dx \int_0^x dy \frac{y}{(Ax + B)(Cx + D)}, \quad \text{(B4)}$$

with

$$A = cy + d, \qquad B = by^2 + ey + f,$$
$$C = (c + h)y + d, \qquad D = (b + j)y^2 + (e + k)y + f. \tag{B5}$$

One changes the integration order as

$$\int_0^1 dx \int_0^x dy = \int_0^1 dy \int_y^1 dx. \tag{B6}$$

We get

$$D_0^{(13)} = \int_0^1 dyy \int_y^1 dx \frac{1}{(Ax + B)(Cx + D)}, \tag{B7}$$

where A, B, C, D are complex. Integrating over x as follows:

$$\int_y^1 dx \frac{1}{(Ax + B)(Cx + D)} = \frac{1}{AC} \int_y^1 \frac{dx}{(x + \frac{B}{A})(x + \frac{D}{C})} = \frac{1}{AD - BC} \int_y^1 \left(\frac{1}{x + \frac{B}{A}} - \frac{1}{x + \frac{D}{C}}\right) dx$$
$$= \frac{1}{AD - BC}\left(\ln\frac{1 + \frac{B}{A}}{y + \frac{B}{A}} - \ln\frac{1 + \frac{D}{C}}{y + \frac{D}{C}}\right) = \frac{1}{AD - BC}\left(\ln\frac{A + B}{Ay + B} - \ln\frac{C + D}{Cy + D}\right), \tag{B8}$$

where we have made sure that the arguments of the logarithms never cross the cut along the negative real axis. One easily gets

$$D_0^{(13)} = \int_0^1 \frac{dy}{(cj - bh)y^2 + (dj + ck - eh)y + dk - fh}\left(\ln\frac{A + B}{Ay + B} - \ln\frac{C + D}{Cy + D}\right). \tag{B9}$$

The discriminant of the quadratic function in the denominator of the prefactor is nothing but the Landau determinant. Indeed,

$$\det Q_4 = (dj + ck - eh)^2 - 4(cj - bh)(dk - fh). \tag{B10}$$

We write

$$D_0^{(13)} = \frac{1}{(cj - bh)(y_2 - y_1)} \int_0^1 \left(\frac{1}{y - y_2} - \frac{1}{y - y_1}\right) \times \left(\ln\frac{A + B}{Ay + B} - \ln\frac{C + D}{Cy + D}\right), \tag{B11}$$

with

$$y_{\frac{1}{2}} = \frac{-(dj + ck - eh) \mp \sqrt{\det Q_4}}{2(cj - bh)}. \tag{B12}$$

Now we have to look at the imaginary parts of the arguments of the logarithms in (B11). We write them explicitly

$$A + B = by^2 + (c + e)y + d + f,$$
$$Ay + B = (b + c)y^2 + (e + d)y + f,$$
$$C + D = (b + j)y^2 + (e + k + c + h)y + d + f,$$
$$Cy + D = (b + j + c + h)y^2 + (e + k + d)y + f. \tag{B13}$$

Imaginary parts read

$$\begin{aligned} \mathrm{Im}\,(A + B) &= \mathrm{Im}(ey + d + f) \\ &= \mathrm{Im}[ym_2^2 + (1 - y)m_3^2 - i\varepsilon] < 0, \\ \mathrm{Im}(Ay + B) &= \mathrm{Im}(ey + dy + f) \\ &= \mathrm{Im}[ym_2^2 + (1 - y)m_4^2 - i\varepsilon] < 0, \\ \mathrm{Im}(C + D) &= \mathrm{Im}[(e + k)y + d + f] \\ &= \mathrm{Im}[ym_1^2 + (1 - y)m_3^2 - i\varepsilon] < 0, \\ \mathrm{Im}(Cy + D) &= \mathrm{Im}[(e + k)y + dy + f] \\ &= \mathrm{Im}[ym_1^2 + (1 - y)m_4^2 - i\varepsilon] < 0. \end{aligned} \tag{B14}$$

Using formula $\ln(a/b) = \ln a - \ln b$ for $\mathrm{Im}(a)\mathrm{Im}(b) > 0$, we rewrite (B11) as

$$D_0^{(13)} = \frac{1}{\sqrt{\det Q_4}} \sum_{i=1}^{2} \sum_{j=1}^{4} (-1)^{i+j} \int_0^1 dy \frac{1}{y - y_i} \times \ln(A_j y^2 + B_j y + C_j), \tag{B15}$$

with

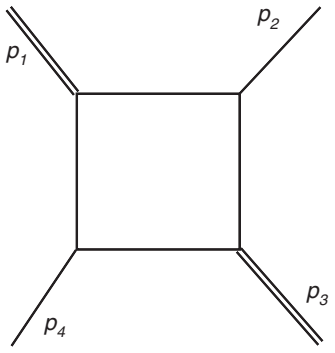

FIG. 17. A box diagram with two opposite lightlike external momenta p_1 and p_3. Double line means massless.

$$A_1 = b + c, \qquad B_1 = e + d, \qquad C_1 = f,$$
$$A_2 = b, \qquad B_2 = c + e, \qquad C_2 = d + f,$$
$$A_3 = b + j, \qquad B_3 = e + k + c + h, \qquad C_3 = d + f,$$
$$A_4 = b + j + c + h, \qquad B_4 = e + k + d, \qquad C_4 = f. \tag{B16}$$

We would like to make an important remark here. From Eq. (B14) we can rewrite Eq. (B11) in the form

$$D_0^{(13)} = \frac{1}{(cj - bh)(y_2 - y_1)} \int_0^1 \left(\frac{1}{y - y_2} - \frac{1}{y - y_1}\right) \times \left(\ln\frac{A + B}{C + D} - \ln\frac{Ay + B}{Cy + D}\right). \tag{B17}$$

We notice that if $y = y_{1,2}$ then $AD = BC$ which means

$$\frac{A + B}{C + D}\bigg|_{y=y_{1,2}} = \frac{Ay + B}{Cy + D}\bigg|_{y=y_{1,2}} = \frac{B}{D}\bigg|_{y=y_{1,2}}. \tag{B18}$$

Thus, we get

$$\int_0^1 \left(\frac{1}{y - y_2} - \frac{1}{y - y_1}\right)\left(\ln\frac{A + B}{C + D}\bigg|_{y=y_{1,2}} - \ln\frac{Ay + B}{Cy + D}\bigg|_{y=y_{1,2}}\right) = 0. \tag{B19}$$

Subtracting this zero contribution from Eq. (B15), we get another form

$$D_0^{(13)} = \frac{1}{\sqrt{\det(Q_4)}} \sum_{i=1}^{2}\sum_{j=1}^{4} (-1)^{i+j} \times \int_0^1 dy \times \frac{\ln(A_j y^2 + B_j y + C_j) - \ln(A_j y_i^2 + B_j y_i + C_j)}{y - y_i} + \frac{1}{\sqrt{\det(Q_4)}} \sum_{i,j=1}^{2} (-1)^{i+j} \eta_{ij} \ln\frac{y_i - 1}{y_i}, \tag{B20}$$

where $\eta_{i1} = \eta(A + B, 1/(C + D))|_{y=y_i}$ and $\eta_{i2} = \eta(Ay + B, 1/(Cy + D))|_{y=y_i}$ with $i = 1, 2$ and the definition of the eta function $\eta(x, y)$ is given in [27]. This representation is more convenient for the evaluation in terms of Spence functions.

Each integral in Eq. (B20) can be written in terms of 4 Spence functions as given in Appendix B of [27]. Thus $D_0^{(13)}$ can be written in terms of 32 Spence functions.

2. Integral with two adjacent lightlike external momenta

For the box shown in Fig. 18 with $p_1^2 = p_2^2 = 0$ one gets $b = g = 0$ and writes

$$D_0^{(12)} = \int_0^1 dx \int_0^x dy \int_0^y dz \frac{1}{(ax^2 + cxy + hxz + jyz + dx + ey + kz + f)^2}. \tag{B21}$$

As in the case of $D_0^{(13)}$, integrating over z gives

$$D_0^{(12)} = \underbrace{\int_0^1 dx \int_0^x dy \frac{1}{a_1 b_1}}_{I_1} + s_k \underbrace{\int_0^1 dx \int_0^x dy \frac{1}{-s_k a_1 (a_1 y + b_1)}}_{I_2}, \tag{B22}$$

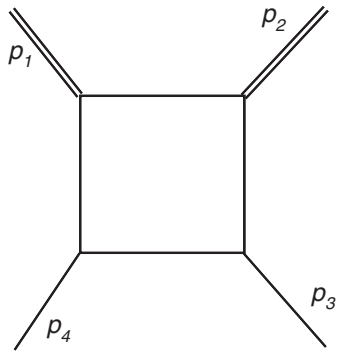

FIG. 18. A box diagram with two adjacent lightlike external momenta p_1 and p_2. Double line means massless.

with

$$s_k = \text{sign}(\text{Im}(k)),$$
$$-s_k a_1 = -s_k(hx + jy + k) - i\varepsilon',$$
$$b_1 = ax^2 + cxy + dx + ey + f,$$
$$a_1 y + b_1 = ax^2 + jy^2 + (c + h)xy + dx + (e + k)y + f - i\varepsilon, \tag{B23}$$

where we have used the fact that $\text{Im}(a_1 y + b_1) = \text{Im}[dx + (e + k)y + f] = \text{Im}[(x - y)m_3^2 + (1 - x)m_4^2 + ym_1^2 - i\varepsilon] < 0$ because $0 \le y \le x \le 1$. ε and ε' are infinitesimal positive quantities which carry the sign of the imaginary parts of $-s_k a_1$ and $a_1 y + b_1$. For I_1, we integrate over y, similar to (B8), to get

$$I_1 = \int_0^1 dy \frac{1}{(ja - hc)y^2 + (jd - he - kc)y + jf - ke} \times \left[\ln\frac{(j + h)y + k - i\varepsilon'}{hy + k - i\varepsilon'} - \ln\frac{(a + c)y^2 + (d + e)y + f}{ay^2 + dy + f}\right]. \tag{B24}$$

Consider the prefactor

$$\det(Q_4) = (jd - he - kc)^2 - 4(ja - hc)(jf - ke),$$
$$y_{11(12)} = \frac{(he + kc - jd) \mp \sqrt{\det(Q_4)}}{2(ja - hc)}, \tag{B25}$$

where the indices 11, 12 correspond to $-$ and $+$ signs, respectively. We rewrite I_1 as

$$\begin{aligned} I_1 &= \frac{1}{\sqrt{\det(Q_4)}} \sum_{i=1}^{2} (-1)^i \int_0^1 dy \frac{1}{y - y_{1i}} \\ &\quad \times \left[\ln \frac{(j + h)y + k - i\varepsilon'}{hy + k - i\varepsilon'} \right. \\ &\quad \left. - \ln \frac{(a + c)y^2 + (d + e)y + f}{ay^2 + dy + f} \right] \\ &= \frac{1}{\sqrt{\det(Q_4)}} \sum_{i=1}^{2} \sum_{j=1}^{4} (-1)^{i+j} \int_0^1 dy \frac{1}{y - y_{1i}} \\ &\quad \times \ln(A_{1j} y^2 + B_{1j} y + C_{1j}), \end{aligned} \tag{B26}$$

with

$$\begin{aligned} &A_{11} = 0, \quad B_{11} = h, \quad C_{11} = k, \\ &A_{12} = 0, \quad B_{12} = j + h, \quad C_{12} = k, \\ &A_{13} = a + c, \quad B_{13} = d + e, \quad C_{13} = f, \\ &A_{14} = a, \quad B_{14} = d, \quad C_{14} = f. \end{aligned} \tag{B27}$$

Thus I_1 can be written in terms of 24 Spence functions. For I_2 we shift $y = y + \alpha x$, α such that

$$j\alpha^2 + (c + h)\alpha + a = 0. \tag{B28}$$

There are, in general, two values of α. The final result does not depend on which value of α we take. We have used this freedom to find bugs in the numerical calculation and it turns out to be a very powerful method to check the correctness of the imaginary part which can be very tricky for the case of equal masses. One gets

$$I_2 = \int_0^1 dx \int_{-\alpha x}^{(1-\alpha)x} dy \frac{1}{(Gx + H - i\varepsilon')(Ex + F - i\varepsilon)}, \tag{B29}$$

with

$$\begin{aligned} &G = -s_k h - s_k j\alpha, \quad H = -s_k jy - s_k k, \\ &E = (2j\alpha + c + h)y + d + \alpha(e + k), \\ &F = jy^2 + (e + k)y + f. \end{aligned} \tag{B30}$$

For real α we have

$$\begin{aligned} \int_0^1 dx \int_{-\alpha x}^{(1-\alpha)x} dy &= \int_0^1 dx \int_0^{(1-\alpha)x} dy - \int_0^1 dx \int_0^{-\alpha x} dy \\ &= \int_0^{1-\alpha} dy \int_{y/(1-\alpha)}^1 dx \\ &\quad - \int_0^{-\alpha} dy \int_{-y/\alpha}^1 dx. \end{aligned} \tag{B31}$$

We write

$$\begin{aligned} &\frac{1}{(Gx + H - i\varepsilon')(Ex + F - i\varepsilon)} \\ &\quad = \frac{1}{GF - HE} \left(\frac{G}{Gx + H - i\varepsilon'} - \frac{E}{Ex + F - i\varepsilon} \right). \end{aligned} \tag{B32}$$

Integrating over x, we get

$$\begin{aligned} I_2 &= \int_{-\alpha}^{1-\alpha} \frac{dy}{GF - HE} \ln \frac{G + H}{E + F} - \int_0^{1-\alpha} \frac{dy}{GF - HE} \\ &\quad \times \ln \frac{\frac{Gy}{1-\alpha} + H}{\frac{Ey}{1-\alpha} + F} + \int_0^{-\alpha} \frac{dy}{GF - HE} \ln \frac{\frac{Gy}{-\alpha} + H}{\frac{Ey}{-\alpha} + F}. \end{aligned} \tag{B33}$$

The prefactor

$$\begin{aligned} \frac{GF - HE}{s_k} &= j(j\alpha + c)y^2 + (2\alpha jk + jd - he + kc)y \\ &\quad + \alpha(ke + k^2 - jf) + kd - hf \\ &= j(j\alpha + c)(y - y_{21})(y - y_{22}), \end{aligned} \tag{B34}$$

with

$$y_{21(22)} = \frac{-(2\alpha jk + jd - he + kc) \mp \sqrt{\det(Q_4)}}{2j(j\alpha + c)}, \tag{B35}$$

where the indices 21, 22 correspond to $-$ and $+$ signs, respectively. We rewrite I_2 as

$$\begin{aligned} I_2 &= \frac{1}{s_k \sqrt{\det(Q_4)}} \sum_{i=1}^{2} (-1)^i I_2^{(i)}, \\ I_2^{(i)} &= \int_{-\alpha}^{1-\alpha} \frac{dy}{y - y_{2i}} \ln \frac{G + H}{E + F} - \int_0^{1-\alpha} \frac{dy}{y - y_{2i}} \ln \frac{\frac{Gy}{1-\alpha} + H}{\frac{Ey}{1-\alpha} + F} \\ &\quad + \int_0^{-\alpha} \frac{dy}{y - y_{2i}} \ln \frac{\frac{Gy}{-\alpha} + H}{\frac{Ey}{-\alpha} + F}. \end{aligned} \tag{B36}$$

We make the substitutions $y = y - \alpha$ for the first integral, $y = (1 - \alpha)y$ for the second integral, and $y = -\alpha y$ for the third integral to get

$$\begin{aligned} I_2^{(i)} &= \int_0^1 \frac{dy}{y - \alpha - y_{2i}} \ln \frac{-s_k jy - s_k h - s_k k - i\varepsilon'}{jy^2 + (c + h + e + k)y + a + d + f - i\varepsilon} - \int_0^1 \frac{(1 - \alpha)dy}{(1 - \alpha)y - y_{2i}} \\ &\quad \times \ln \frac{-s_k(j + h)y - s_k k - i\varepsilon'}{(a + c + j + h)y^2 + (d + e + k)y + f - i\varepsilon} + \int_0^1 \frac{-\alpha dy}{-\alpha y - y_{2i}} \ln \frac{-s_k hy - s_k k - i\varepsilon'}{ay^2 + dy + f - i\varepsilon}. \end{aligned} \tag{B37}$$

Consider the arguments of the three logarithms, as demonstrated in (B14), it is easy to see that the sign of the imaginary parts of the denominators is negative as indicated by $-i\varepsilon$. The derivation is for real α. However, this result can be easily generalized to cover the case of complex α as shown below. We can now rewrite I_2 as

$$I_2 = \frac{1}{s_k\sqrt{\det(Q_4)}} \sum_{i=1}^{2}\sum_{j=1}^{6}(-1)^i \int_0^1 dy \frac{c_j}{a_j y - b_j - y_{2i}} \ln(A_{2j}y^2 + B_{2j}y + C_{2j}), \tag{B38}$$

with

$$\begin{aligned}
&c_1 = 1, \quad a_1 = 1, \quad b_1 = \alpha, \quad c_2 = -(1-\alpha), \quad a_2 = 1-\alpha, \quad b_2 = 0,\\
&c_3 = -\alpha, \quad a_3 = -\alpha, \quad b_3 = 0, \quad c_4 = -1, \quad a_4 = 1, \quad b_4 = \alpha,\\
&c_5 = 1-\alpha, \quad a_5 = 1-\alpha, \quad b_5 = 0, \quad c_6 = \alpha, \quad a_6 = -\alpha, \quad b_6 = 0,\\
&A_{21} = 0, \quad B_{21} = -s_k j, \quad C_{21} = -s_k k - s_k h, \quad A_{22} = 0, \quad B_{22} = -s_k(j+h), \quad C_{22} = -s_k k,\\
&A_{23} = 0, \quad B_{23} = -s_k h, \quad C_{23} = -s_k k, \quad A_{24} = j, \quad B_{24} = c + h + e + k, \quad C_{24} = a + d + f,\\
&A_{25} = a + c + j + h, \quad B_{25} = d + e + k, \quad C_{25} = f, \quad A_{26} = a, \quad B_{26} = d, \quad C_{26} = f.
\end{aligned} \tag{B39}$$

I_2 can be written in terms of 36 Spence functions. Thus

$$D_0^{(12)} = I_1 + s_k I_2 \tag{B40}$$

contains 60 Spence functions. For the evaluation of $D_0^{(12)}$ in terms of Spence functions and to generalize Eq. (B38) for complex α, we have to do the following replacement for each logarithm in $I_{1,2}$:

$$\begin{aligned}
\ln(A_{1j}y^2 + B_{1j}y + C_{1j}) &\to \ln(A_{1j}y^2 + B_{1j}y + C_{1j})\\
&\quad - \ln(A_{1j}y_{1i}^2 + B_{1j}y_{1i} + C_{1j}),\\
\ln(A_{2j}y^2 + B_{2j}y + C_{2j}) &\to \ln(A_{2j}y^2 + B_{2j}y + C_{2j})\\
&\quad - \ln(A_{2j}\hat{y}_{2i}^2 + B_{2j}\hat{y}_{2i} + C_{2j}),
\end{aligned} \tag{B41}$$

with $\hat{y}_{2i} = (y_{2i} + b_j)/a_j$, and add the corresponding extra terms related to the eta functions. The argument for this is similar to that explained in the previous section; see Eq. (B20).

For the boxes with one lightlike external momentum, the result is written in terms of 72 Spence functions by using exactly the same method.

APPENDIX C: SINGULARITIES OF THE THREE-POINT FUNCTION

In the main text, we concentrated on the properties of the four-point one-loop function especially as concerns the occurrence of the leading Landau singularity which in that case is not integrable. Although a leading singularity in the three-point function is integrable, it is instructive to study the case of the three-point function in some detail as it sheds light on some properties we unravelled in the four-point function. Moreover the three-point function appears also when shrinking or collapsing one of the internal lines into a point and therefore its singularities are part of the singularities of the corresponding four-point function. The study of the three-point scalar integral is easier to handle as it involves less parameters. We take as an example, the three-point loop integral shown in Fig. 19 that is part of the diagrams contributing to class (c).

In terms of the Passarino-Veltman appellation, this scalar integral writes

$$\begin{aligned}
T_0^3(s_2) &= C_0(s_2, M_H^2, 0, m_t^2, M_W^2, M_W^2),\\
s_2 &= (p_4 + p_5)^2.
\end{aligned} \tag{C1}$$

The bottom-quark mass has been neglected by setting it to 0. The phase-space constraint on s_2 is $M_H^2 \le s_2 \le s$; see Eq. (13).

We will define the Landau determinant, $\det Q_3$, corresponding to a three-point function, $C_0(p_1^2, p_2^2, p_3^3, m_1^2, m_2^2, m_3^2)$ according to the Passarino-Veltman notation

$$\det Q_3(p_1^2, p_2^2, p_3^3; m_1^2, m_2^2, m_3^2) \tag{C2}$$

with m_i the internal masses and p_i^2 the invariants of the external momenta. In the same spirit the determinant of a two-point function will be defined as

$$\begin{aligned}
\det Q_2(p^2; m_1^2, m_2^2) &= -\lambda(p^2; m_1^2, m_2^2)\\
&= -(p^2 - (m_1 + m_2)^2)\\
&\quad \times (p^2 - (m_1 - m_2)^2),
\end{aligned} \tag{C3}$$

where $\lambda(a, b, c)$ is the usual kinematic function; see Eq. (15). For completeness and later reference, the determinant of the one-point function is defined as

$$\det Q_1(m^2) = 2m^2. \tag{C4}$$

A necessary condition for a three-point function to have a LLS is that it has exactly two cuts which can produce physical on shell particles. The diagram in Fig. 19 satisfies this condition when

$$M_H \ge 2M_W \quad \text{and} \quad \sqrt{s_2} \ge m_t + M_W. \tag{C5}$$

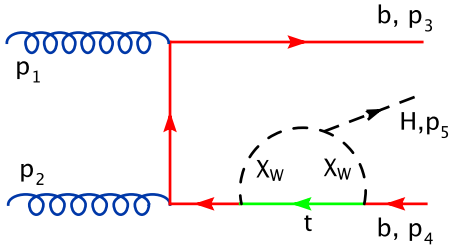

FIG. 19 (color online). A triangle diagram contributing to $gg \to b\bar{b}H$ that can develop a leading Landau singularity for $M_H \geq 2M_W$ and $\sqrt{s_2} \geq m_t + M_W$, i.e. all the three particles in the loop can be simultaneously on shell.

These conditions are part of the conditions for our four-point function (that we studied in Sec. III) to have an LLS. In fact, this three-point function is a reduced diagram from the point of view of our four-point function where it is considered as a subleading Landau singularity. These conditions Eq. (C5) represent the opening up of normal thresholds. We will refer to the first threshold $M_H \geq 2M_W$ as the Higgs threshold ($H \to W^+W^-$), while the second condition will be referred to as the s_2 threshold ($Hb \to Wt$). The sign condition ($x_i > 0$), Eq. (8) for the case at hand, is particularly simple here. For example,

$$\begin{aligned} \det\hat{Q}_{13} &= -M_H^2(m_t^2 + M_W^2) + 2s_2M_W^2 \leq 0, \\ \det\hat{Q}_{23} &= -M_H^2(m_t^2 + M_W^2) + s_2(M_H^2 - 2M_W^2) \leq 0, \end{aligned} \tag{C6}$$

which together with Eq. (C5) give

$$s_2 \leq \frac{M_W^2 + m_t^2}{M_H^2 - 2M_W^2}M_H^2 \leq 2(m_t^2 + M_W^2). \tag{C7}$$

These inequalities are supplemented by the condition of vanishing Landau determinant in order for the appearance of the LLS. The Landau determinant in our case is

$$\begin{aligned} \det Q_3(s_2, M_H^2) &\equiv \det(s_2, M_H^2, 0; m_t^2, M_W^2, M_W^2) \\ &= -2M_W^2s_2^2 + 2M_H^2(m_t^2 + M_W^2)s_2 \\ &\quad - 2M_H^2(M_H^2m_t^2 + (m_t^2 - M_W^2)^2). \end{aligned} \tag{C8}$$

We have chosen to pick up s_2 as the variable in which to study the location of the LLS, hence our notation $\det Q_3(s_2, M_H^2)$. It is very rewarding to express this determinant in terms of a perfect square in s_2 plus a remainder which is the discriminant of the quadratic equation. We can then write

$$\begin{aligned} \det Q_3(s_2, M_H^2) &= -\det Q_1(m_t^2) \\ &\quad \times \left((s_2 - s_2^0)^2 - \frac{\det Q_2^0}{\det Q_1(m_t^2)}\frac{\det Q_2^{M_H^2}}{Q_1(m_t^2)}\right) \\ \text{with} \quad \det Q_2^{M_H^2} &= \det Q_2(M_H^2; M_W^2, M_W^2), \\ \det Q_2^0 &= \det Q_2(0; m_t^2, M_W^2), \end{aligned} \tag{C9}$$

$$s_2^0 = 2(m_t^2 + M_W^2) + (M_H^2 - 4M_W^2)\left(1 + \frac{m_t^2 - M_W^2}{2M_W^2}\right). \tag{C10}$$

It is important to note that the discriminant is the product of two subdeterminants, independent of s_2, corresponding to 2 two-point functions each one obtained by collapsing or shrinking one of the internal lines bringing one vertex of the original three-point function to coincide with the "s_2 vertex", s_2 in which we write the perfect square. This is a general theorem [22] that applies to symmetric matrices based on the Jacobi ratio theorem for determinants [23].

The roots $s_{2,\pm}$ (from $\det Q_3(s_2, M_H^2) = 0$) give the position of the LLS as a function of M_H, for fixed m_t, M_W. In view of the constraint Eq. (C7) only one solution is possible. It is given by

$$\begin{aligned} s_2^H &= s_2^{\mathrm{LLS}} \\ &= \frac{1}{2M_W^2}(M_H^2(M_W^2 + m_t^2) \\ &\quad - (m_t^2 - M_W^2)M_H\sqrt{M_H^2 - 4M_W^2}) \\ &= s_2^0 - \frac{m_t^2 - M_W^2}{2M_W^2}M_H^2\sqrt{1 - 4M_W^2/M_H^2}. \end{aligned} \tag{C11}$$

The surface that defines Eq. (C11) is the surface of the LLS region. This surface is bounded, however, due to the constraint from the inequalities due to the normal thresholds and the sign condition. This is what defines the region of the LLS singularity. In fact, the normal thresholds are directly related to the range of the LLS region. First of all, if $M_H < 2M_W$ there is no LLS. At exactly the Higgs threshold, $M_H = 2M_W$ and $\det Q_2^{M_H^2} = 0$, the LLS according to Eq. (C11) occurs at $s_2^{\mathrm{LLS}} = 2(m_t^2 + M_W^2)$ which is the *maximum* value of s_2 given by Eq. (C7). When M_H increases, the value of s_2^{LLS} decreases until s_2 reaches the s_2 threshold, $(m_t + M_W)^2$, below which the LLS disappears. Therefore the s_2 threshold, via the vanishing of the Landau determinant will give the maximum value of M_H for the appearance of the LLS. We therefore find that the region of the LLS is delimited as

$$\begin{aligned} &4M_W^2 \leq M_H^2 \leq 4M_W^2 + \frac{M_W}{m_t}(m_t - M_W)^2, \\ &(m_t + M_W)^2 \leq s_2 \leq 2(m_t^2 + M_W^2). \end{aligned} \tag{C12}$$

Numerically, this corresponds to

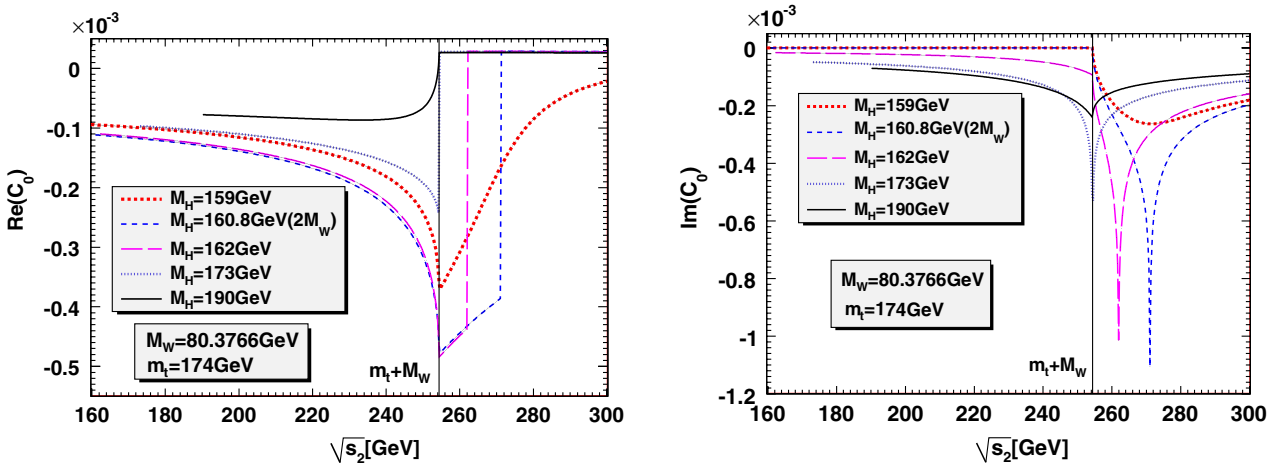

FIG. 20 (color online). Left panel: the real part of C_0 as a function of $\sqrt{s_2}$ with various values of M_H. Right panel: the same plots for the imaginary part.

$$160.75\ \text{GeV} \leq M_H \leq 172.89\ \text{GeV},$$
$$254.38\ \text{GeV} \leq \sqrt{s_2} \leq 271.06\ \text{GeV}. \tag{C13}$$

This range in the variables M_H, s_2 can be derived in a much simpler way. The Landau constraint of vanishing determinant $\det Q_3(s_2, M_H^2)$ is a surface. This is bounded by tangents parallel to the coordinate variables [22], s_2, M_H^2 so that with m_t and M_W fixed, these extrema are given by

$$\begin{aligned}\frac{\partial \det Q_3(s_2, M_H^2)}{\partial s_2} &= 0 \Rightarrow s_2^{\text{ext}} = s_2^0 \Rightarrow \det Q_2^{M_H^2} \\ &= 0 (\text{since} \det Q_3(s_2, M_H^2) = 0) \Rightarrow M_H \\ &= 2M_W \Rightarrow s_2^{\text{extr.1}} = 2(m_t^2 + M_W^2).\end{aligned} \tag{C14}$$

The other extrema are derived in a similar way by considering

$$\begin{aligned}\frac{\partial \det Q_3(s_2, M_H^2)}{\partial M_H^2} &= 0 \Rightarrow \det Q_2^{s_2} = 0 \Rightarrow s_2^{\text{extr.2}} \\ &= (m_t + M_W)^2 \Rightarrow M_H^2 \\ &= 4M_W^2 + \frac{M_W}{m_t}(m_t - M_W)^2.\end{aligned} \tag{C15}$$

It is crucially important to observe that these extrema do correspond to normal thresholds where a leading singularity and a subleading singularity coincide. This feature will be carried through to the case of the four-point function.

The location of the singularity, as well as its range, is well rendered in Fig. 20 which shows how the location of the LLS moves as we vary the Higgs mass. Figure 20 shows both the real and imaginary part of scalar three-point function. Note that as shown in Sec. III, here the LLS is of a logarithm type. This explains why one observes a jump, a step function discontinuity, in the real part and a logarithmic singularity in the imaginary part or vice versa. We see that for $M_H = 159\ \text{GeV} < 2M_W$, a funnel develops at the normal s_2 threshold for the real part while the imaginary part develops a nonzero value past this threshold with a rather smooth and broad structure. For $M_H = 2M_W$, at the Higgs threshold, the imaginary part develops are very sharp dip at $s_2 = 2(m_t^2 + M_W^2)$ which is furthest from the normal s_2 threshold at $s_2 = (m_t + M_W)^2$. As the Higgs mass increases, this sharp dip moves to the left towards the normal s_2 threshold beyond which the sharp peaks signalling the LLS disappear leaving only a *dent* at the normal (s_2) threshold.

[1] A. Djouadi, Phys. Rep. **457**, 1 (2008).
[2] N. E. Adam *et al.*, arXiv:0803.1154.
[3] R. M. Barnett, H. E. Haber, and D. E. Soper, Nucl. Phys. **B306**, 697 (1988); D. A. Dicus and S. Willenbrock, Phys. Rev. D **39**, 751 (1989); D. Dicus, T. Stelzer, Z. Sullivan, and S. Willenbrock, Phys. Rev. D **59**, 094016 (1999); C. Balazs, H. J. He, and C. P. Yuan, Phys. Rev. D **60**, 114001 (1999); R. V. Harlander and W. B. Kilgore Phys. Rev. D **68**, 013001 (2003); S. Dittmaier, M. Krämer, and M. Spira, Phys. Rev. D **70**, 074010 (2004); S. Dawson, C. B. Jackson, L. Reina, and D. Wackeroth, Phys. Rev. D **69**, 074027 (2004); G. Gao, R. J. Oakes, and J. M. Yang, Phys. Rev. D **71**, 095005 (2005); S. Dawson, C. B. Jackson, L. Reina, and D. Wackeroth, Mod. Phys. Lett. A **21**, 89 (2006); W. Hollik and M. Rauch, AIP Conf. Proc. **903**, 117 (2007); S. Dittmaier, M. Kramer, A. Muck, and

T. Schluter, J. High Energy Phys. 03 (**2007**) 114; S. Dawson and C. B. Jackson, Phys. Rev. D **77**, 015019 (2008).
[4] F. Boudjema and D. N. Le, Phys. Rev. D **77**, 033003 (2008).
[5] L. D. Landau, Nucl. Phys. **13**, 181 (1959).
[6] R. J. Eden, P. V. Landshoff, D. I. Olive, and J. C. Polkinghorne, *The Analytic S-matrix* (Cambridge University Press, Cambridge, England, 1966).
[7] A. Denner, S. Dittmaier, and T. Hahn, Phys. Rev. D **56**, 117 (1997).
[8] Z. Nagy and D. E. Soper, Phys. Rev. D **74**, 093006 (2006); T. Binoth, G. Heinrich, T. Gehrmann, and P. Mastrolia, Phys. Lett. B **649**, 422 (2007); G. Ossola, C. G. Papadopoulos, and R. Pittau, J. High Energy Phys. 07 (2007) 085; C. Bernicot and J. P. Guillet, J. High Energy Phys. 01 (2008) 059.
[9] A. Freitas, A. von Manteuffel, and P. M. Zerwas, Eur. Phys. J. C **34**, 487 (2004).
[10] W. Hou and R. G. Stuart, Phys. Rev. D **43**, 3669 (1991).
[11] Z. Bern *et al.*, arXiv:0803.0494.
[12] G. J. van Oldenborgh and J. A. M. Vermaseren, Z. Phys. C **46**, 425 (1990).
[13] T. Hahn and M. Perez-Victoria, Comput. Phys. Commun. **118**, 153 (1999).
[14] S. Dawson, C. B. Jackson, L. Reina, and D. Wackeroth, Phys. Rev. D **69**, 074027 (2004).
[15] K. A. Assamagan *et al.* (Higgs Working Group Collaboration), arXiv:hep-ph/0406152.
[16] S. Dittmaier, M. Krämer, and M. Spira, Phys. Rev. D **70**, 074010 (2004).
[17] R. Kleiss and W. J. Stirling, Nucl. Phys. **B262**, 235 (1985); A. Ballestrero and E. Maina, Phys. Lett. B **350**, 225 (1995).
[18] J. C. Polkinghorne and G. R. Screaton, Nuovo Cimento **15**, 925 (1960).
[19] S. Coleman and R. E. Norton, Nuovo Cimento **38**, 438 (1965).
[20] T. Binoth, M. Ciccolini, N. Kauer, and M. Kramer J. High Energy Phys. 03 (2005) 065.
[21] D. N. Le, arXiv:0810.4078.
[22] J. Tarski, J. Math. Phys. (N.Y.) **1**, 149 (1960).
[23] H. W. Turnbull, *The Theory of Determinants, Matrices ans Invariants* (Dover Publications, Inc., New York, 1960).
[24] J. Cunningham, Rev. Mod. Phys. **36**, 833 (1964).
[25] A. Denner and S. Dittmaier, Nucl. Phys. **B658**, 175 (2003).
[26] T. Hahn and M. Rauch, Nucl. Phys. B, Proc. Suppl. **157**, 236 (2006).
[27] G. 't Hooft and M. Veltman, Nucl. Phys. **B153**, 365 (1979).
[28] F. Boudjema, A. Semenov, and D. Temes, Phys. Rev. D **72**, 055024 (2005).
[29] E. de Doncker, Y. Shimizu, J. Fujimoto, F. Yuasa, K. Kaugars, L. Cucos, and J. Van Voorst, Nucl. Instrum. Methods Phys. Res., Sect. A **534**, 269 (2004).E. de Doncker, Y. Shimizu, J. Fujimoto, and F. Yuasa, Comput. Phys. Commun. **159**, 145 (2004).Y. Yasui *et al.*, arXiv:0710.2957.
[30] A. Denner, J. Küblbeck, R. Mertig, and M. Böhm, Z. Phys. C **56**, 261 (1992).B. A. Kniehl, Z. Phys. C **55**, 605 (1992).See also, J. Fleischer and F. Jegerlehner, Nucl. Phys. **B216**, 469 (1983).G. Belanger, F. Boudjema, J. Fujimoto, T. Ishikawa, T. Kaneko, K. Kato, and Y. Shimizu, Phys. Lett. B **559**, 252 (2003).
[31] T. Bhattacharya and S. Willenbrock, Phys. Rev. D **47**, 4022 (1993); K. Melnikov, M. Spira, and O. Yakovlev, Z. Phys. C **64**, 401 (1994); B. A. Kniehl, C. P. Palisoc, and A. Sirlin, Nucl. Phys. **B591**, 296 (2000).
[32] http://user.pa.msu.edu/wkt/cteq/cteq6/cteq6pdf.html.
[33] J. Pumplin *et al.*, J. High Energy Phys. 07 (2002) 012.
[34] D. Stump *et al.*, J. High Energy Phys. 10 (2003) 046.
[35] S. Kretzer, H. L. Lai, F. I. Olness, and W. K. Tung, Phys. Rev. D **69**, 114005 (2004).
[36] A. Denner, U. Nierste, and R. Scharf, Nucl. Phys. **B367**, 637 (1991).